

MECHANISMS OF CYTOMEGALOVIRUS REGULATION OF
NEURODEGENERATIVE MARKERS

A DISSERTATION

SUBMITTED IN PARTIAL FULFILLMENT OF THE REQUIREMENTS

FOR THE DEGREE OF DOCTOR OF PHILOSOPHY

IN THE GRADUATE SCHOOL OF THE

TEXAS WOMAN'S UNIVERSITY

DEPARTMENT OF BIOLOGY

COLLEGE OF ARTS AND SCIENCES

BY

PRAPTI MODY B.S., M.S.

DENTON, TEXAS

AUGUST 2019

Copyright © 2019 by Prapti Mody

DEDICATION

I dedicate this dissertation to Kushal. Thank you for making me stronger and always believing in me.

ACKNOWLEDGMENTS

I would like to extend heartfelt gratitude to Dr. Juliet Spencer for her timely advice regarding my dissertation project. I greatly appreciate my co-mentors Dr. Laura Hanson and Dr. DiAnna Hynds, who stood with me through all the highs and lows. I would like to thank my committee members for their insights that ultimately made my work better. I thank Dr. Shazia Ahmed for her understanding and support through the past 7 years. I appreciate the late Dr. Sarah McIntire, who granted me admission into the program and nominated me for Phi Kappa Phi membership. I thank the Quality Enhancement Program Grant committees at TWU for granting me monetary awards for my research and teaching projects, as part of the Experiential Learning Student Scholar Program. I thank the TWU Alumni Association for awarding me the 2019 TWU Outstanding Graduate Student Award and recognizing my accomplishments.

I thank Dr. Jay Reddy at AIT Labs for employment through my dissertation writing months.

To my friends, colleagues and acquaintances, I extend many thanks for always being there as commiserates and for their constant moral support.

To my family, especially Kushal, words are inadequate for expressing how grateful I am for your emotional support.

ABSTRACT

PRAPTI MODY

MECHANISMS OF CYTOMEGALOVIRUS REGULATION OF NEURODEGENERATIVE MARKERS

AUGUST 2019

Alzheimer's disease (AD) manifests with loss of neurons associated with intercellular amyloid plaques made up of amyloid beta peptides (A β) and intracellular neurofibrillary tangles of hyperphosphorylated tau proteins.¹ Normally, A β peptides function as cell signaling molecules and can mediate antimicrobial activity.²⁻⁴ Tau is one of the microtubule stabilizing proteins in cells and its expression and post-translational modifications depend upon cell type and cell age.⁵⁻⁸

Despite testing many therapeutics designed to target abnormal amyloid or tau, there is no sustained treatment.^{9,10} Current research is therefore focused on early steps in production of dysfunctional amyloid and tau¹¹, however, there are relatively few strong established models for these studies.

Previous researchers have shown that some herpesvirus infections can alter amyloid and tau in ways similar to that seen in AD.¹²⁻¹⁶ There is clinical correlation between herpesvirus infection and higher risk of AD.¹⁶⁻¹⁸ Herpes simplex virus 1 can interact with amyloid precursor protein (APP)^{19,20} and affect tau hyperphosphorylation.

^{14,15} Based on these findings, we hypothesized that MCMV infection could be a useful model if it similarly impacts AD markers.

We found that APP was upregulated in MCMV-infected fibroblasts and viral late gene products were required. Levels of processing enzymes (secretases) and one cleavage product (A β 42) were unchanged. The activity of β -secretase was not increased. There was no similar APP induction in RCN. Thus, CMV may have cell-type or species-based differences for effects on the amyloid pathway.

Levels of total tau and tau phosphorylated at S396 were increased in MCMV-infected fibroblasts and neurons. This also required viral late gene products. There was no change in tau phosphorylation at S202 or GSK3 β levels. We used lithium chloride (LiCl) to inhibit activity of GSK3. Although MCMV infection was inhibited, the banding patterns for tau and phospho-tau (S396) exhibited minor alterations when LiCl was added at the time that changes started. Thus, other kinases are more likely important.

We have confirmed that MCMV can induce AD markers. This is useful for using MCMV infection in AD animal models for elucidation of early steps, promising for testing novel preventives for these changes, and for developing novel antivirals.

TABLE OF CONTENTS

| | Page |
|-------------------------------------------------------|------|
| DEDICATION | ii |
| ACKNOWLEDGMENTS | iii |
| ABSTRACT..... | iv |
| LIST OF TABLES | viii |
| LIST OF FIGURES | ix |
| ABBREVIATIONS | x |
| Chapter | |
| I. INTRODUCTION..... | 1 |
| Neurodegeneration..... | 1 |
| Alzheimer’s disease | 1 |
| Amyloid beta peptide | 2 |
| Hyperphosphorylated tau | 6 |
| Crosstalk between amyloid and tau pathways | 10 |
| Herpesviruses | 12 |
| Cytomegalovirus..... | 13 |
| Herpesviruses and neurodegeneration | 15 |
| Model | 17 |
| II. MATERIALS AND METHODS | 18 |
| Cell culture..... | 18 |
| Virus maintenance, infection and UV inactivation..... | 19 |
| Western blots | 20 |
| Viral late gene inhibition studies | 24 |

| | |
|-----------------------------------------------------------------|----|
| ELISA for secreted A β 42 | 24 |
| Fluorometric assay for β -secretase activity | 25 |
| Viral binding/entry studies..... | 25 |
| Northern blots | 27 |
| Immunofluorescence..... | 28 |
| Inhibition of GSK3 activity by LiCl | 29 |
| Statistical analyses | 30 |
| III. RESULTS..... | 31 |
| Rat neuronal cells are permissive for MCMV infection | 31 |
| Effects of MCMV infection upon the amyloid pathway..... | 34 |
| Results in mouse NIH3T3 fibroblasts..... | 34 |
| Results in rat neuronal cells | 44 |
| Effects of MCMV infection upon tau and its phosphorylation..... | 46 |
| Results in mouse NIH3T3 fibroblasts..... | 46 |
| Results in primary rat cortical neurons | 56 |
| IV. DISCUSSION | 63 |
| MCMV and amyloid..... | 64 |
| MCMV and tau | 67 |
| REFERENCES | 72 |
| APPENDICES | 84 |
| A. Levels of APP in rat B35 neuroblastomas..... | 84 |
| B. Levels of PS2 in primary RCN..... | 86 |
| C. Immunoblotting analysis of A β 42..... | 88 |
| D. Northern blot analysis | 91 |
| E. Tau and its phosphorylation in rat B35 cells..... | 94 |

LIST OF TABLES

| Table | Page |
|---------------------------------------------------------------------------|------|
| 1. The known human herpesviruses, their classification, and diseases..... | 12 |
| 2. Information about antibodies used in this dissertation..... | 22 |
| 3. Conditions used for antibody incubations..... | 23 |

LIST OF FIGURES

| Figure | Page |
|----------------------------------------------------------------------------------------------------------------------|------|
| 1. APP processing | 3 |
| 2. Hypotheses for overproduction of amyloid beta peptides in CNS | 6 |
| 3. Tau hyperphosphorylation in Alzheimer's disease-associated tauopathy | 8 |
| 4. Different hypotheses for tau modifications leading to tau aggregation | 10 |
| 5. Schematic representation of a CMV virion | 13 |
| 6. Experiment setup diagram for viral binding and entry study | 26 |
| 7. Experiment setup for GSK3 inhibition by lithium chloride (LiCl) | 29 |
| 8. Rat neuronal cells are permissive for MCMV infection..... | 33 |
| 9. APP is induced during MCMV infection in mouse fibroblasts | 35 |
| 10. MCMV infection increases levels of the 90 and 120 kDa APP isoforms..... | 36 |
| 11. Viral late gene expression is necessary for induction of APP levels in fibroblasts. | 37 |
| 12. Levels of secreted A β 42 are not affected by MCMV infection in fibroblasts | 39 |
| 13. Levels of PS2 in fibroblasts remain unchanged with MCMV infection..... | 40 |
| 14. Analyses of β -secretase levels in NIH3T3 fibroblasts during MCMV infection | 41 |
| 15. Activity of β -secretase is reduced in MCMV-infected fibroblasts | 43 |
| 16. MCMV infection in primary rat cortical neurons does not induce changes in APP levels | 45 |
| 17. Total tau is induced upon MCMV infection in fibroblasts..... | 47 |
| 18. Representative western blots for demonstration of successful MCMV infection and foscarnet treatment..... | 48 |
| 19. Viral late gene expression is necessary for tau induction..... | 49 |
| 20. Viral binding and entry is not sufficient to induce total tau levels in fibroblasts | 51 |
| 21. Phosphorylation of tau at serine 396 is induced at late times during CMV infection | 52 |
| 22. Viral late gene products are required for induced phosphorylation of tau at S396, in fibroblasts..... | 54 |
| 23. MCMV infection does not affect phosphorylation of tau at serine 202 in fibroblasts | 55 |
| 24. Tau and its phosphorylation at S396 and S202 is affected in a similar manner in primary RCN | 57 |
| 25. MCMV infection does not affect levels of GSK3 β in fibroblasts | 59 |
| 26. Inhibition of GSK3 from onset of MCMV infection has very little effect on total tau and phospho-tau S396..... | 60 |
| 27. MCMV is inhibited by LiCl | 62 |
| 28. Proposed model of MCMV interactions with amyloid and tau pathways of neurodegeneration | 64 |
| 29. MCMV infection does not induce APP in rat B35 neuroblastomas | 85 |
| 30. Levels of PS2 in RCN during MCMV infection | 87 |
| 31. Secreted A β 42 peptide detection via western blotting | 90 |
| 32. Northern blot analysis of total RNA isolated from MCMV-infected fibroblasts | 93 |
| 33. Rat B35 neuroblastomas have induced tau during MCMV infection..... | 95 |
| 34. Tau phosphorylation in rat B35 neuroblastoma cells..... | 96 |

ABBREVIATIONS

AD Alzheimer's disease
ANOVA analysis of variance
APP amyloid precursor protein
A β amyloid beta peptide
A β 40 amyloid beta peptide (1-40)
A β 42 amyloid beta peptide (1-42)
BACE1 beta amyloid cleaving enzyme 1, beta secretase 1
BCS bovine calf serum
BSA bovine serum albumin
CMV cytomegalovirus
CNS central nervous system
DMEM Dulbecco's modified eagle medium
FBS fetal bovine serum
HCMV human cytomegalovirus
HPI hours post infection
HSV-1 herpes simplex virus 1
LiCl lithium chloride
LSD least significant difference
MCMV murine cytomegalovirus, mouse cytomegalovirus
PBS phosphate buffered saline
PNS peripheral nervous system
PS2 presenilin 2, gamma secretase active subunit
SDS sodium dodecyl sulfate
WB western blot

CHAPTER I INTRODUCTION

NEURODEGENERATION

Neurodegeneration refers to a decline in cognitive function due to a gradual loss of neuronal cells.²¹ Neurodegeneration has many different underlying mechanisms. These include but are not restricted to genetic mutations (sometimes causing inherited neurodegenerative diseases), infections, stimulation of apoptosis, and oxidative damage.²² A similarity on the subcellular level in most of the mechanisms is the accumulation of misfolded or abnormally modified cellular proteins and/or failure to remove mislocalized, toxic protein/peptide aggregates. These aggregates can spread across cells to cause progressive impairment of nervous system functioning.²² This dissertation focuses on Alzheimer's disease-specific neurodegeneration markers and the hypothesis that chronic infection is a contributing factor to onset or acceleration of neurodegenerative pathology.

ALZHEIMER'S DISEASE

Alzheimer's disease (AD) is the third leading cause of death for the geriatric population in the United States.²³ The main symptom of AD is dementia that is precipitated by a gradual loss of neurons. There are two hallmark pathologies associated with AD - intercellular deposits of amyloid peptides that form insoluble plaques and intracellular accumulation of abnormally phosphorylated tau proteins that form neurofibrillary tangles of paired helical filament structures.²³

Amyloid Beta Peptide

Aggregation-prone amyloid peptides are abnormal cleavage products of the amyloid precursor protein (APP).²⁴ This precursor is a transmembrane protein that is usually cleaved by α -secretase, followed by γ -secretase (non-amyloidogenic pathway – Figure 1) to generate normal amyloid-beta (A β) peptides that act as signaling molecules between neuronal cells to maintain synapses and communication.²⁵ There is increasing evidence for A β peptides also having direct antimicrobial activity and ability to elicit an immune response by binding to receptors on microglia and activating them.^{2-4,26}

In AD, APP is cleaved by β -secretase (BACE1) followed by γ -secretase, which generates a longer peptide called amyloid-beta 42 (A β 42).²⁷ This peptide, along with other longer amyloid peptides, can form insoluble plaques between neurons in the brain that disrupt synapses.²⁷ This is called the amyloidogenic pathway (Figure 1). These peptides may also have antimicrobial activity.^{3,4,26}

Experimental evidence has suggested that levels of soluble amyloid peptides as well as diffuse plaque structures impair cognition by interfering with synaptic functions, and that insoluble oligomers of amyloid peptides are apparent at a later stage of AD.²⁸⁻³¹ Intracellular A β has been shown to localize in microvesicles that are trafficked to neuron synapses and an overproduction of these peptides was associated with synaptic dysfunction.³²

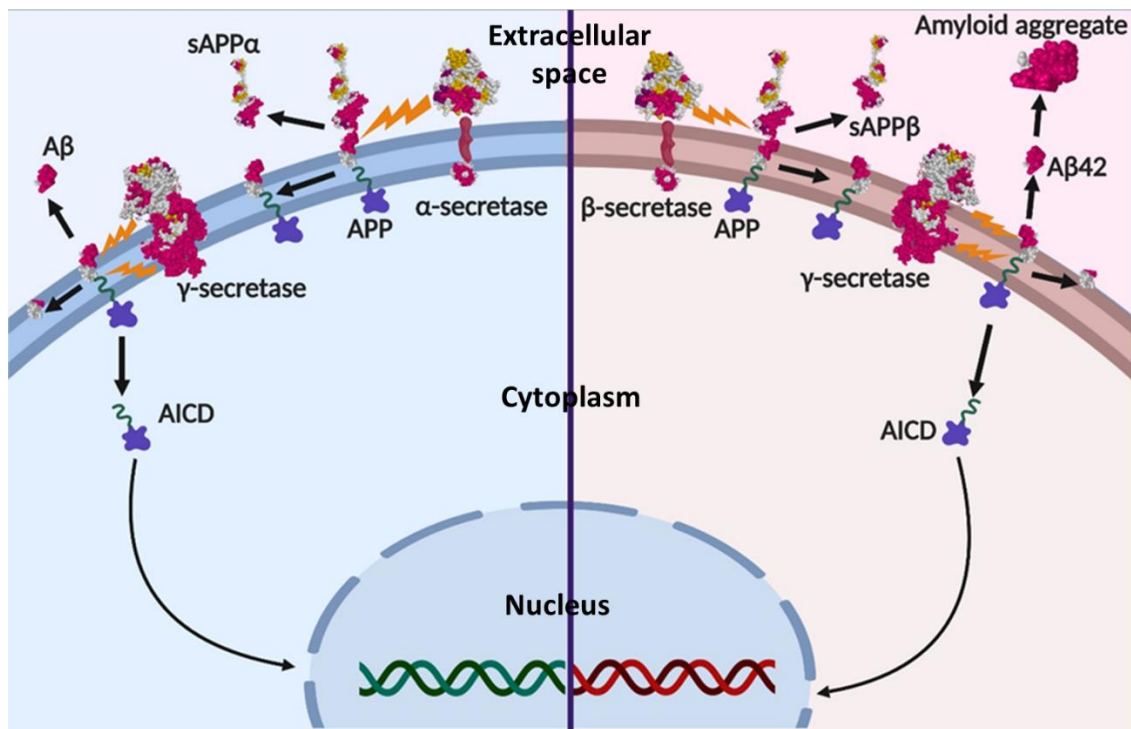


Figure 1. APP processing. Non-amyloidogenic processing of APP by α -secretase followed by γ -secretase pathway shaded in light blue. Amyloidogenic processing of APP by β -secretase followed by γ -secretase pathway shaded in light pink. Images were generated using Biorender software. Protein structure models were imported from the Protein Data Bank (PDB). PDB IDs: APP - 1mw6, 1owt, 1rw6, 1iyt; β -secretase – 1sgz, 1py1; γ -secretase – 5A63).

There are numerous transcripts produced from the APP gene in mammals³³ of which 3-4 are protein-encoding. Three predominant protein isoforms of full-length APP called APP770, APP751, and APP695 are translated from 3 alternatively spliced variants of the APP transcript.³⁴ Their molecular weights range from ~90 to ~130 kilodaltons (kDa).³⁵ All 3 isoforms are variants of the secreted soluble APP (sAPP α or sAPP β).³⁶ All isoforms are processed by the same pathway and can generate A β peptides.

The APP695 isoform is known to be predominantly expressed in the central nervous system (CNS) whereas the other two are more ubiquitously expressed.^{27,37} The

APP is made up of an extracellular, a transmembrane, and an intracellular region.³⁸ The N-terminal extracellular region contains a copper binding domain, growth-factor-like domain, an acidic domain, and a serine protease inhibitor domain.³⁹ This extracellular portion of APP is usually cleaved by α or β -secretases and the remaining transmembrane and intracellular domains are then cleaved by γ -secretase.³⁹ The APP695 isoform lacks a protease inhibitor domain in its extracellular portion which is found in the larger isoforms.³⁹ The higher molecular weight APP770 and APP751 have more bulky posttranslational modifications like glycosylation, sialylation, and tyrosine sulfation compared to APP695.³⁶

The α -secretase is a transmembrane enzyme known to cleave APP within the A β peptide sequence generating a secreted N-terminal soluble APP fragment (sAPP α) and a transmembrane C-terminal fragment (AICD).⁴⁰ It has been published that overexpression of α -secretase leads to reduced production of longer, aggregation-prone A β peptides.⁴⁰ However, α -secretase mediated cleavage has been shown to produce fragments of C-terminal APP that have been found in diffuse plaques.²⁸

The β -secretase enzyme is an aspartic protease also referred to as β -site APP cleaving enzyme 1 (BACE1). This enzyme is mainly localized in endosomal membranes, is highly expressed in neurons, and requires a lower pH for activity compared to α -secretase.⁴⁰ Another enzyme called BACE2 is believed to be an isoform of BACE1 because it shares 64% amino acid homology with BACE1.⁴¹ It is expressed more in non-neuronal cells and can contribute to production of A β from APP by glial cells.⁴²

The γ -secretase is a multiprotein enzyme complex that is responsible for cleavage of the APP transmembrane portion following the action of α or β secretases. The catalytic core is made up of two proteins, presenilin 1 and 2 (PS1, PS2). This core is surrounded by accessory proteins nicastrin, anterior pharynx defective 1 (APH1), and presenilin enhancer protein 2 (PEN2)⁴³ which are involved in stabilization of the complex.⁴⁴

Generation of A β 42 and longer peptides, via β and γ -secretase cleavage, leads to formation of insoluble plaques.⁴⁵ These longer peptides are more aggregation-prone due to addition of charged amino acids at the C-terminus, rather than shorter versions.⁴⁵ However, there is ample evidence that normal aging brains have amyloid aggregates that are not arranged in insoluble beta-pleated sheets.^{31,45-48} These soluble aggregates are not pathological but have the potential to seed plaque formation.⁴⁵ Amyloid aggregates in people without dementia have also been linked with low memory between 70 and 90 years of age³⁰, but not necessarily cognitive decline. All this evidence points to a poor correlation between insoluble amyloid plaques being causative for AD dementia. Figure 2 shows various hypotheses for overproduction of amyloid beta, leading to pathological amyloid peptides.

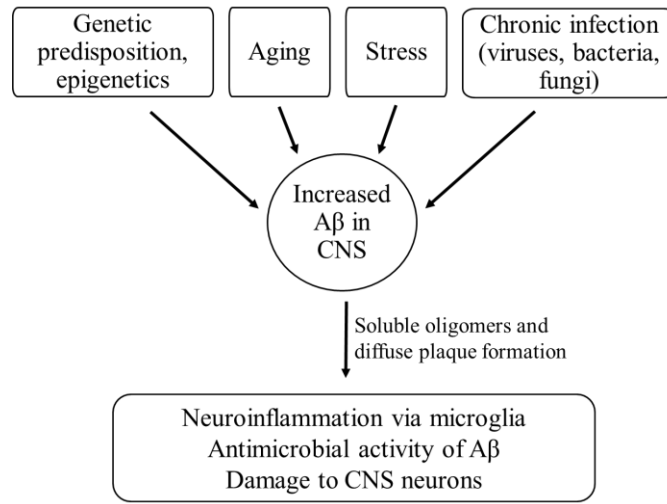


Figure 2. Hypotheses for overproduction of amyloid beta peptides in CNS. Different genetic and environmental factors may act separately or in concert to upregulate production of amyloid beta peptides. These may, in turn, set off inflammation pathways that cause damage to the neuronal cells. ^a

The early steps leading to increased intracellular or secreted A β that contribute to cognitive decline have not been elucidated. There is also evidence for the amyloid pathology originating in CNS cells like glia or astrocytes and spreading to neurons in the aging brain. ⁴⁹ Therapeutics for reducing/inhibiting β -secretase activity, improving cognition via neurotransmitters, or addressing late-stage disease have not led to sustained treatment. ⁹ Hence, it is important to investigate early steps that lead to production of dysfunctional amyloid peptides.

Hyperphosphorylated Tau

Tau stabilizes microtubules within cells, including along axons of neurons. ⁶

Microtubules are cytoskeletal structures made up of heterodimers of α and β -tubulin

^a Adapted from Figure 1 of Fulop T, Witkowski JM, Bourgade K, et al. Can an Infection Hypothesis Explain the Beta Amyloid Hypothesis of Alzheimer's Disease? *Front Aging Neurosci.* 2018;10:224.

proteins.⁵⁰ Formation of microtubules starts with $\alpha\beta$ tubulin dimers being arranged on γ -tubulin at the microtubule organizing center. The microtubules are highly dynamic and undergo polymerization and depolymerization based on cellular environment.⁵⁰ There are a number of proteins called microtubule associated proteins (MAPs) that help keep the microtubule structure stable.⁵⁰ Tau is one such MAP.⁵⁰

The levels of tau protein expression and tau localization are dependent upon cell type as well as cell age. For example, in immature neurons, tau is localized in the cell body and neurites but in mature neurons, it is more axonal.⁶ Tau also varies in phosphorylation status when bound along axons.⁵¹

Tau is divided into 2 domains structurally: the projection domain that comprises two-thirds of the protein from the amino terminus and the microtubule-binding domain that comprises the remaining one-third towards the carboxyl terminus.⁵² There are 6 isoforms of tau normally expressed in the adult human brain and all have varied post-translational modifications like acetylation, phosphorylation, glycosylation, and ubiquitination.⁵³ Without post-translational modifications, the 6 isoforms of tau range in size between 35 and 46 kDa.⁵⁴ While predominant expression of tau in the CNS has been documented in the literature, newer analyses have shown that it is also expressed in non-neuronal brain cells at lower levels and reduced phosphorylation.^{7,51,55}

In AD, tau proteins become abnormally hyperphosphorylated and dissociate from the microtubules to form neurofibrillary tangles (Figure 2) that are not cleared by the proteasome.⁵² In non-mitotic brain cells, tau has been shown to induce formation of

paired helical filaments via impaired degradation by the proteasome.⁵⁶ Tau hyperphosphorylation is a consequence of upregulation of kinases and/or a downregulation in cellular phosphatases.⁶ This not only interferes with intracellular signaling and trafficking, but also leads to a collapse of the cellular cytoskeleton transport mechanisms, leading to neuron death.^{8,54,57}

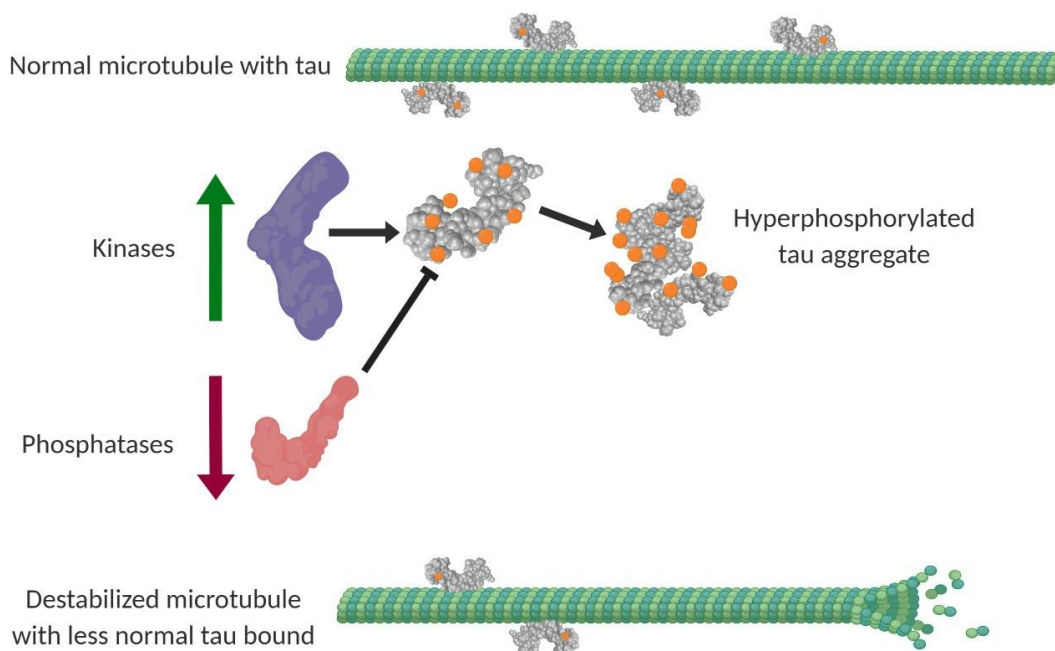


Figure 3. Tau hyperphosphorylation in Alzheimer’s disease-associated tauopathy. Tau proteins are normally found along microtubules in axons of neurons where they function to stabilize them. In AD, an upregulation of kinases (upward pointing green solid arrow) and/or downregulation of phosphatases (downward pointing dark red solid arrow) has been reported to cause tau hyperphosphorylation. Abnormally modified tau falls off the microtubules and aggregates in insoluble paired helical filaments in the cytoplasm leading to microtubule instability and collapse as well as interference with normal cellular functions. Images were generated using Biorender software. Tau structure model was imported from the Protein Data Bank (PDB). PDB ID: tau – 1j1c.

All tau isoforms can be phosphorylated at more than 70 sites. Most of these are outside the microtubule binding domains, with the exception of ~6 sites within microtubule binding domains.⁵² Cellular kinases like glycogen synthase kinase 3 alpha and beta (GSK3 α and GSK3 β), protein kinase A (PKA), mitogen-activated protein kinase (MAPK), cyclin dependent kinase 5 (CDK5), and eukaryotic initiation factor two alpha kinase (eIF2AK), among others, are involved in tau phosphorylation during normal physiological as well as neurodegenerative disease conditions.^{58,59} The key kinases implicated in AD-associated tau dysregulation are GSK3, CDK5, and PKA.^{58,60,61} Hyperactivity of kinases has also been shown to increase translation of tau transcripts generating more total tau which may indicate a cellular mechanism to compensate for loss of microtubule-bound tau.⁵⁹

Phosphorylation of tau is carefully controlled in cells by a balance between kinase and phosphatase activity. Tau dephosphorylation is primarily carried out by protein phosphatase 2A and 2B (PP2A and PP2B).⁶² In neurodegenerative diseases presenting with tau aggregations (tauopathies), abnormal hyperphosphorylation is evident along with a decrease in phosphatase activity.⁶³ A decrease in phosphatase activity of these enzymes can be mediated by ApoE protein encoded by the apolipoprotein E ϵ 4 allele.⁶⁴ The ApoE protein was shown to downregulate PP2A transcription as well as methylation of its catalytic subunit, leading to reduced PP2A activity.⁶⁴ Thus, increased activity of kinases and/or decreased phosphatase activity can result in tau hyperphosphorylation.

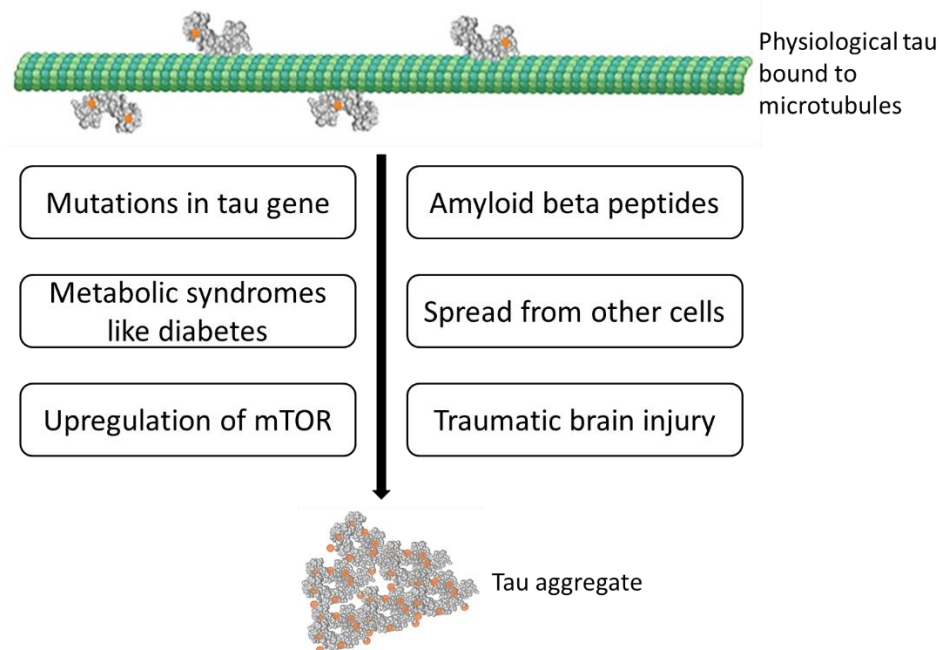


Figure 4. Different hypotheses for tau modifications leading to tau aggregation. Various mutations, metabolic pathway disruption, and other factors contribute to cause tau hyperphosphorylation. This causes abnormal tau to fall off the microtubules and aggregate. ^b

Crosstalk between the Amyloid and Tau Pathways

There are multiple studies showing that A β peptides can influence tau phosphorylation dysregulation. ⁶⁵⁻⁶⁸ An overproduction of A β peptides was shown to induce aggregation-prone tau species even before formation of A β plaques. ⁶⁵ The resultant aggregation-prone tau was shown to be capable of seeding and spreading this pathology. ⁶⁵

Another study has shown that A β 42, rather than A β 40, has greater activity in promoting tau cleavage, phosphorylation, and aggregation *in vitro*. ⁶⁷ The presence of the

^b Adapted from Figure 1 of Orr ME, Sullivan AC, Frost B. A Brief Overview of Tauopathy: Causes, Consequences, and Therapeutic Strategies. Trends Pharmacol Sci. 2017;38(7):637–648.

apoE4 allele was shown to be a contributing factor in the presence of tau hyperphosphorylation whereas the apoE3 allele (not involved in AD-related A β pathology) did not make a difference.⁶⁹

There is evidence that phosphorylation of APP and tau can be brought about by A β via GSK3 β and cdk5.⁶⁸ In this study, phosphorylation of APP was shown to regulate its own production, and subsequently, the production of A β , which then led to tau phosphorylation at serine 262 and 396 via GSK3 and cdk5.⁶⁸

On the other hand, the evidence for hyperphosphorylated tau leading to A β toxicity is sparse.⁷⁰⁻⁷² Tau phosphorylation by MAPK p38 at threonine 205 was shown to reduce A β toxicity by disruption of A β signaling via N-methyl-D-aspartate (NMDA) type glutamate receptors.⁷³ A reduction in endogenous tau levels was shown to confer neuroprotective effects against A β -mediated toxicity.^{71,72} Thus, there is evidence as to how the amyloid and tau pathways may be linked, but how dysregulation of one may lead to the other being disrupted, is still not clear. There is a need for finer dissection of early stages in mechanisms leading to these pathologies and the available AD animal models have yielded few insights.

Since amyloid beta functions as an antimicrobial peptide,^{2-4,26} chronic infections of the CNS can trigger its overproduction. Herpesviruses have the ability to go latent following primary infection, can reactivate multiple times, and establish lifelong infections in their hosts. Thus, they can be a good chronic infection model to study induction of amyloid beta in various AD animal models.

HERPESVIRUSES

Herpesviruses are ubiquitous in the human population.⁷⁴ These are large, dsDNA viruses known to establish latency with periodic reactivation in their host.⁷⁵

Herpesviruses have co-evolved with their hosts. Mammalian herpesviruses are classified into α , β , and γ -herpesvirus families based upon evolutionary divergence and characterization whereas avian and reptilian herpesviruses are all believed to be α -herpesviruses.⁷⁶ A hallmark of herpes viruses is that they can establish lifelong latency within their host cells and are capable of reactivation when the immune system is compromised for example, during pregnancy, illness, aging, or stress.⁷⁷ Table 1 lists the nine human herpes viruses with their information.

Table 1. The known human herpesviruses, their classification, and diseases.

| Classification | Name | Latency in cells | Common disease examples |
|----------------|------------------------------------------------|------------------|---------------------------------------------|
| α | Herpes simplex 1 (HSV-1) | Neurons | Oral herpes |
| | Herpes simplex 2 (HSV-2) | | Genital herpes |
| | Varicella zoster (VZV) | | Chicken pox, shingles |
| β | Human cytomegalovirus (HCMV) | Myeloid cells | Mononucleosis, retinitis |
| | Human herpesvirus 6A (HHV-6A) | | <i>Roseola infantum</i> , pityriasis rosea |
| | Human herpesvirus 6B (HHV-6B) | | |
| | Human herpesvirus 7 (HHV-7) | | |
| γ | Epstein barr (EBV) | B cells | EBV-associated lymphoproliferative diseases |
| | Kaposi's sarcoma-associated herpesvirus (KSHV) | | Kaposi's sarcoma |

CYTOMEGALOVIRUS

Cytomegalovirus (CMV) is a member of the β -herpesvirus family. These viruses have a limited host range compared to α -herpesviruses, have a longer reproductive cycle, and can establish latent infection in cells of secretory glands, endothelial systems, and kidneys.⁷⁷ Human CMV (HCMV) infects 60-100% of adults worldwide, depending upon region and socio-economic status.¹⁸ Primary infection with CMV occurs by close contact of epithelial surfaces with infected bodily fluids. The virus disseminates through innate effector cells to various organs and can also spread cell-to-cell.⁷⁸ Primary infection and reactivation are usually asymptomatic in individuals with a robust immune system.⁷⁷

Figure 5 shows a schematic of CMV structure.

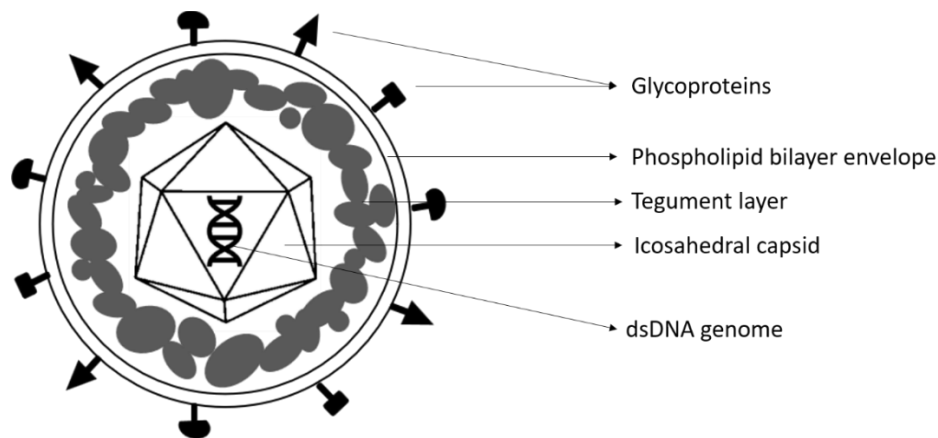


Figure 5. Schematic representation of a CMV virion. The dsDNA genome is enclosed in an icosahedral protein capsid that is surrounded by a multi-protein layer called the tegument. This whole particle is then encased in a lipid bilayer membrane with surface glycoproteins that help the virus dock onto cells and enter.

The viral particle packs a genome of ~235 kb dsDNA genome within an icosahedral protein capsid. Herpesvirus genomes contain genes that are categorized into

three kinetic classes.⁷⁹ The first class is immediate-early (IE) genes that are transcribed once the viral DNA is inside the host cell nucleus. *De novo* viral gene expression is not required for transcription of IE genes. These encode many viral transcription factors. Then, the early (E) genes are expressed that encode proteins required for viral DNA replication, among others. This step is followed by replication of viral genomes. The last kinetic class of genes is then expressed, and these are classified as late (L) genes. Many of these late genes encode structural proteins needed for the viral capsids and viral tegument proteins.⁷⁹ Viral genome replication is the prerequisite step for expression of late genes.⁸⁰

The viral capsid is surrounded by a multilayered, highly organized structure of viral tegument proteins that have a variety of functions in viral entry, capsid transport to the nucleus, virion assembly, and egress (Figure 5).⁸¹ The tegument is encased in a phospholipid bilayer envelope containing viral glycoproteins that are necessary for binding to host cell surface receptors for entry.⁷⁸

The replication cycle starts when infectious viral particles bind to host cell surface receptors using their glycoproteins and enter by fusion of their envelope with a host cell membrane. Once inside the cytoplasm, the tegument layer is dissociated, and the capsids are trafficked to the nucleus via microtubules where the viral genomes are injected inside the nucleus through nuclear pores.⁸² In some cells, there are morphological changes associated with viral infection. Infected cells become rounded up and fuse together to

form multinucleate cells termed as syncytia.⁸³ This is called the cytopathic effect and indicates viral infection as it requires expression of viral genes.

HERPESVIRUSES AND NEURODEGENERATION

There is clinical correlation between presence of various herpes viruses and neurodegeneration.^{13,84,85} DNA from herpes simplex virus 1 (HSV-1), herpes simplex virus 2 (HSV-2), HCMV, and human herpes virus 6B (HHV-6B) has been found localized within plaques in AD patient brains.^{17,84} More recently, genomes of human herpesvirus 6A (HHV-6A) and human herpes virus 7 (HHV-7), have also been reported in AD patients' brains, but this investigation did not examine whether these genomes were specifically localized to plaques.⁸⁶

Herpes simplex virus 1 infects progenitor cells of the CNS readily and can infect mature neurons and astrocytes but needs a higher concentration of the virus particles to do so.⁸⁷ Various studies have shown direct HSV-1 interactions with APP.^{14,20} HSV-1 infection was found to alter the subcellular localization of APP and HSV-1 capsids directly interacted with AD markers.^{14,15,19,20} There is also evidence that HSV-1 infection causes A β to localize in autophagic compartments and inhibits the non-amyloidogenic pathway for APP processing.⁸⁸

Wozniak et al have demonstrated that HSV-1 infection can induce AD-associated tau hyperphosphorylation at various sites.¹⁴ Current antivirals against HSV-1 can reverse this pathology in tissue culture.¹⁵ Thus, the virus can induce markers associated with AD pathologies *in vitro*.

Infection of mice and rabbits with HSV-1 is possible; however, it is unlike the natural human host system.^{89,90} *In vivo* studies upon cohorts infected with HSV-1 are difficult as the virus can establish lifelong infection, without symptoms. Evidence from HSV-1 infection of human cells has been used to start clinical trial for testing antivirals as neurodegeneration preventives.⁹¹

CMV can cause congenital infection, go latent and can reactivate during various stresses.^{12,18,92} No direct or indirect mechanisms have been published for CMV and its role in neurodegeneration despite a clear association with neuropathogenesis (60-90% children infected *in utero* show long-term neurological sequelae).¹² CMV is known to infect neural progenitor cells, astrocytes, and immature neurons, among other neuronal cell types.¹²

Lurain et al published that A β 42 staining was increased in HCMV-infected human fibroblasts in tissue culture at a single time point after infection, as part of a larger study that analyzed clinical correlation between HCMV and AD-specific amyloid pathology.¹⁶ However, the mechanisms were not addressed. We have not found any studies regarding CMV and tau. Strong evidence for presence of herpesvirus genomes in AD patients' brains along with known mechanisms of HSV-1 upregulating amyloid and tau pathologies, warrants investigation into whether CMV infection similarly affects neurodegenerative disease markers. If this outcome is positive, it would provide another system to examine the early steps that may lead to neurodegeneration.

MODEL

Experiments using HCMV in human systems pose ethical challenges. HCMV cannot productively infect rodents. Instead, using the murine cytomegalovirus (MCMV) model has many advantages. Mouse CMV has similar kinetics to HCMV, encodes many proteins homologous to those of HCMV, and produces a number of similar pathologies in its natural rodent host.⁹³ MCMV is also known to infect both mice and rats⁹⁴ which can be valuable to applying findings from tissue culture to mice and rat models of AD. We have used murine CMV infection in NIH3T3 fibroblasts, rat B35 neuroblastomas, and primary rat cortical neurons to investigate if amyloid and tau modifications, associated with AD, are altered. We have demonstrated permissivity of the rat neuronal cells for MCMV infection, analyzed steady-state levels of target proteins, and analyzed activity of key enzymes involved in dysregulated amyloid and tau pathways, in tissue culture. Our hypothesis was that MCMV will upregulate APP, A β 42, tau and tau phosphorylation. We tried to answer the following 3 broad questions through the work presented in this dissertation:

- 1) What cellular factors (pertaining to AD pathways) are affected during MCMV infection?
- 2) What kinetic class of viral factors is involved?
- 3) Investigate findings from fibroblasts in primary cortical neurons.

CHAPTER II

MATERIALS AND METHODS

CELL CULTURE

Murine NIH3T3 fibroblasts (ATCC® CRL-1658™) were maintained in Dulbecco's modified Eagle's medium (DMEM) (Gibco-Life Technologies, MD) supplemented with 10% bovine calf serum (BCS - Atlanta Biologicals, GA).⁹⁵ Cells were split every third day by trypsinization when 3×10^5 cells per 75 cm^2 area were seeded into a fresh flask of DMEM-10% BCS and the remaining cells were used to set up experiments. This regimen was strictly followed, and cells were used between passages 133 and 160 (with 128 being the earliest passage available from ATCC).

Rat B35 neuroblastoma cells (ATCC CRL-2754™) were maintained in DMEM/F12 media (Gibco-Life Technologies, MD) supplemented with 10% fetal bovine serum (FBS - Atlanta Biologicals, GA).⁹⁶ These were split by trypsinization when confluent in 75 cm^2 flasks and subsequently seeded for experiments or into new flasks for maintenance. Cells were used between passages 4 and 22.

Rat primary cortical neurons were obtained from newborn brain tissue (Hynds lab, TWU). Postnatal day 1 rat pup brains were dissected into 1 mm slices, meninges were removed, and cortices isolated. Papain digestion was performed at 37°C for 30 minutes, stopped by addition of FBS, and tissue was further dissociated via a fire-polished glass Pasteur pipette. The homogenized cell suspension was diluted with

DMEM-10% FBS and put on 60 mm dishes or on chambered slides at an approximate density of 2 to 4×10^5 cells/well. Media was changed to neurobasal (Gibco-Life Technologies, MD) supplemented with B-27 mitosis inhibitor (Thermo-Fisher Scientific, Waltham, MA), and glutamine (Invitrogen, Waltham, MA) after 4 hours for selectively culturing primary neurons. These were used for infections and assays within 3 weeks post plating.

VIRUS MAINTENANCE, INFECTION, AND UV-INACTIVATION

Preparation of MCMV Stocks

The Smith strain of MCMV (ATCC VR 194) was used for all infections. All virus stocks were prepared using NIH3T3 cells. One plaque-forming unit (PFU) per 10000 cells was inoculated into a 75 cm^2 flask of 75-80% confluent NIH3T3 cells. This was incubated at 37°C for 1 hour punctuated by rocking every 15 minutes. The inoculum was then removed and DMEM with 5% BCS was added. The flask was incubated at 37°C with 5% CO_2 until 80% of the cells showed cytopathic effect (rounded multinucleate cells – syncytia formation), after which it was frozen at -80°C for at least 15 minutes followed by thawing to room temperature (RT) to break open cells and release cell-associated virus. The suspension was centrifuged at $500 \times g$ for 10 minutes to pellet cell debris and the clarified supernatant was aliquoted into 1 ml cryovials. These were stored frozen at -80°C and one vial was thawed for quantification of infectious virus titer by standard plaque assay.⁹⁷

Infection of Cells with MCMV

For MCMV infection, cells were seeded onto appropriate dishes or chambered slides and allowed to stabilize for 24 hours. Cells were inoculated with MCMV at a multiplicity of infection (MOI) of 2 PFU/cell and kept at 37°C for 1 hour punctuated with rocking every 15 minutes. The inoculum was then removed, and fresh media was added. Cells and/or media were immediately harvested for time points 0-no virus and 0 hours post infection (HPI). The difference between these samples was that the 0-no virus cells were incubated with media without virus for the 1 hour of inoculation whereas the 0 HPI sample cells were inoculated with media containing MCMV for the hour of inoculation. This was considered time 0 for all infected or mock-infected cells.

Preparation of Inactivated MCMV by UV Treatment

A fresh MCMV stock was divided in half. One half of the MCMV stock was aliquoted into cryovials. The other half was poured into a sterile 200 mm petri dish and subjected to 200 kJ/cm² of UV irradiation for 2 minutes in a UV crosslinker (Stratagene). The solution was gently swirled to mix and irradiated again for 2 minutes at the same dose. This was then aliquoted into cryovials. Both sets of cryovials were stored at -80°C until titering and use.

WESTERN BLOTS

Sample Collection and Lysate Preparation

Cells were seeded in 60 mm tissue culture dishes at 5 x 10⁵ cells/dish and allowed to stabilize for 24 hours at 37°C in a humidified 5% CO₂ incubator. These were then

infected with MCMV at a MOI of 2 PFU/cell. Cell lysates were prepared in western lysis buffer (50 mM Tris, 1% sodium dodecyl sulfate-SDS, pH 7.5) at specified time points and the ratio used was 200 μ l buffer for every 1×10^6 cells.

Lysate Analyses

Total protein was quantitated in all cell lysates using the Bio-Rad DC protein assay kit that is compatible with SDS (Bio-Rad, Hercules, CA, Cat. no. 5000112). Equal amount of protein (10 or 20 μ g) was loaded onto 10-12% SDS-polyacrylamide gels, depending on proteins being analyzed. Denaturing gels were run for 45 to 65 minutes at 200 V at RT in SDS running buffer (25 mM Tris, 192 mM glycine, 0.1% SDS, pH 8.3) and proteins were transferred to nitrocellulose or polyvinylidene fluoride (PVDF) membranes overnight at 15-30 volts in transfer buffer (25 mM tris, 192 mM glycine, pH 8.5). If proteins being analyzed were 75 kDa or larger, the transfer buffer was supplemented with 20% methanol to enhance transfer and binding to membranes.

Western Blotting

The membranes were air dried to enhance protein binding and re-wet in deionized water before blocking with 5% nonfat dry milk. Bovine serum albumin (BSA - Dot Scientific Inc. Cat. no. DSA30075-100) at 5%, was used for rabbit-anti-A β 1-42 primary antibody dilution only. The milk or BSA was dissolved in tris-buffered saline/tween-20 (TBST) solution (50 mM Tris, 150 mM sodium chloride, 0.05% Tween-20, pH 7.5) to make block buffer. Blocking was done for 1 hour at room temperature on a rocker.

Membranes were probed with appropriate primary and secondary antibodies for detection of target proteins and loading-control proteins. See Table 2 for general information on all antibodies used and table 3 for information on temperatures and incubation times for all antibodies used. Membranes were washed 3 times with TBST after each primary and secondary antibody incubation.

Table 2. Information on antibodies used in this dissertation. WB – western blot, IF – immunofluorescence.

| Antibody | Dilution | Company |
|-----------------------------------------|---------------------|-----------------------------|
| Mouse anti α -tubulin | 1:5000 | |
| Mouse anti β -actin | 1:5000 | |
| Rabbit anti tau | 1:1000 | Sigma-Aldrich |
| Goat anti rabbit FITC conjugate | 1:200 | |
| Goat anti mouse TRITC conjugate | 1:200 | |
| Rabbit anti amyloid precursor protein | 1:5000 | |
| Rabbit anti tau phospho S202 | 1:1000 | Abcam |
| Rabbit anti BACE1 | 1:1000 | |
| Rabbit anti PS2 | 1:1000 | |
| Rabbit anti tau phospho S396 | 1:1000 | Novus Biologicals |
| Rabbit anti amyloid beta (1-42) peptide | 1:1000 | Cell Signaling Technologies |
| Goat anti rabbit CW 800 | 1:15000 | LiCor |
| Goat anti mouse IRDye 680 | 1:15000 | |
| Rabbit anti E1 | 1:1000 WB, 1:200 IF | |
| Rabbit anti major capsid protein | 1:1000 | Laura Hanson, Ph.D. |
| Rabbit anti m143 | 1:1000 | |

Table 3. Conditions used for antibodies. All antibodies were diluted in 5% nonfat dry milk made up in tris-buffered saline unless marked with *. All incubations were carried out on rockers except for antibodies used for immunofluorescence that are marked with #. RT – room temperature, WB – western blot, IF – immunofluorescence.

| Antibody | Incubation time | Incubation temperature |
|----------------------------------------------|--------------------------|-------------------------------|
| Mouse anti α -tubulin | ≥ 1 hour | RT |
| Mouse anti β -actin | ≥ 1 hour | RT |
| Rabbit anti tau | 3 hours | RT |
| Goat anti rabbit FITC conjugate [#] | 1 hour | RT (dark) |
| Goat anti mouse TRITC conjugate [#] | 1 hour | RT (dark) |
| Rabbit anti amyloid precursor protein | 3 hours | RT |
| Rabbit anti tau phospho S202 | Overnight (12-16 hours) | 4°C |
| Rabbit anti β -secretase | 3 hours | RT |
| Rabbit anti PS2 | 2 hours | RT |
| Rabbit anti tau phospho S396 | 3 hours | RT |
| Rabbit anti amyloid beta (1-42) peptide* | Overnight (12-16 hours) | 4°C |
| Mouse anti β III tubulin [#] | Overnight (12-16 hours) | 4°C |
| Goat anti rabbit CW 800 | 1 hour | RT |
| Goat anti mouse IRDye 680 | 1 hour | RT |
| Rabbit anti E1 | 1 hour | RT |
| Rabbit anti major capsid protein | 1 hour, WB 1 hour, IF | RT, WB 37°C, IF |
| Rabbit anti m143 | 1hour | RT |

Detection and Band Analyses

Detection was done on a LiCor Odyssey CLx using Image Studio software. For all western blots that showed multiple bands depicting target protein isoforms, images were imported into the Image Lab software (BioRad) and analyzed using scanning densitometry to generate intensity values as areas under the curve. The intensities of each

target protein band were normalized against loading control band intensities (β -actin or α -tubulin). After normalization, each lane was compared to the 0-no virus lane to get fold change values.

VIRAL LATE GENE INHIBITION STUDIES

Viral genome replication is essential for expression of viral late genes for herpesviruses. Foscarnet (phosphonoformic acid - PFA) is an established MCMV replication inhibitor.⁹⁸ This was used at a working concentration of 300 μ g/ml of media in a set of uninfected and infected NIH3T3 and RCN. Cell lysates were prepared, and western blots were performed as described in the section on western blots.

ELISA FOR SECRETED A β 42

The levels of secreted amyloid beta peptide (A β 42) were assayed by ELISA (My Bio Source, San Diego, Cat. No. MBS265825 for mouse samples and MBS067517 for rat samples). These are sandwich-based ELISA kits that use a monoclonal antibody coated onto wells of a plate to bind A β 42 in samples. The bound A β 42 is detected by another anti-A β 42 polyclonal antibody conjugate targeted to a different epitope. Media from cultures of uninfected or infected fibroblasts with/without foscarnet and similarly from primary neurons was collected at 48, and 72 HPI and stored at -80°C until use – this is referred to as conditioned media henceforth. The cells were plated and infected as described in the section for virus maintenance and infection. Conditioned media (100 μ l volume) was directly used for ELISA according to kit protocols. Samples were run in triplicate. To subtract background, control wells with fresh media that has not been exposed to cells,

were set up in addition to the blank wells, which got only kit substrate, enzyme, detector solution, and stop solution. After adjusting values for blank, the media background well readings were subtracted from sample readings for better background subtraction.

FLUOROMETRIC ASSAY FOR ACTIVITY OF β -SECRETASE

The activity of β -secretase enzyme was measured in fibroblasts by the beta-secretase fluorometric assay kit (Abcam, Cambridge, MA, ab65357). Cells were plated, infected and treated as described in the section for viral late gene inhibition experiments. Cell lysates were prepared in kit extraction buffer at 0, 12, 24, 48, and 72 HPI. The cells were rinsed twice with ice-cold PBS and homogenized in 100 μ l kit extraction buffer by pipetting thrice using a 10-100 μ l micropipette. Samples were clarified by centrifugation at 15,000 x g for 5 minutes at 4°C and clarified supernatants used for the assay according to kit protocol. Briefly, 50 μ l of clarified supernatant was pipetted into the wells and kit substrate was added to all wells. Negative control wells received the kit inhibitor. The kit β -secretase enzyme was added to the positive and negative control wells. The plate was incubated at 37°C for 30 minutes and fluorescence was detected on a BIO-TEK Synergy plate reader. Total protein was estimated in all samples by the Bio-Rad DC protein assay kit (Bio-Rad, Hercules, CA, Cat. no. 5000112) and was used to normalize fluorescence intensities.

VIRAL BINDING/ENTRY STUDIES

Murine NIH3T3 fibroblasts were infected with wildtype (WT) virus or UV-inactivated virus. The WT virus had a titer of 5.5×10^5 PFU/ml whereas the matched UV-

inactivated virus titer was 98 PFU/ml. NIH3T3 cells were seeded on 60 mm dishes at 5×10^5 cells/dish and allowed to stabilize for 24 hours. Mock infected, WT infected, and UV-inactivated virus treated samples were set up. Following the hour of incubation, the inoculum was removed, and cells were washed twice with acid-glycine buffer (0.1 M glycine, pH 3) to remove loosely bound virus.⁹⁵ Cell lysates were prepared at 72 HPI and subjected to western blots for total tau protein, and viral markers as described in the section on western blots.

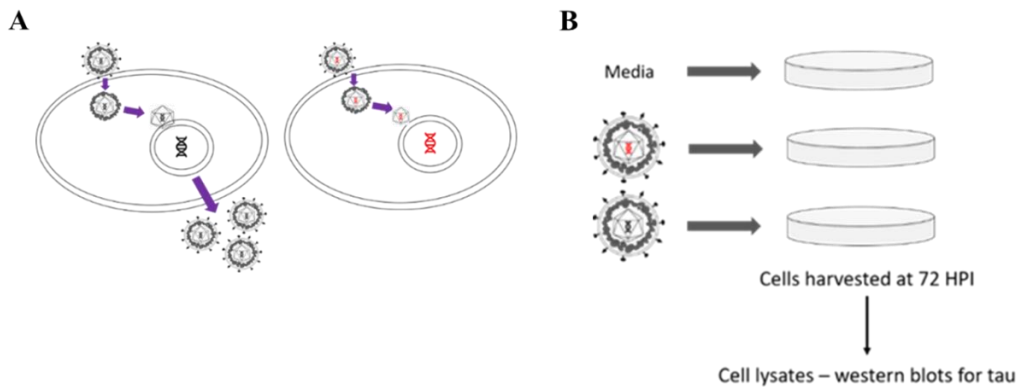


Figure 6. Experiment setup diagram for viral binding and entry study. (A) Schematic representation - normal WT MCMV can enter cells and undergo complete replication cycle whereas UV-inactivated MCMV can enter but lacks gene expression so cannot undergo complete replication cycle. The virus with red DNA depicts UV-inactivated MCMV and the virus with gray DNA depicts WT MCMV. (B) Experiment setup - plates were incubated with respective virus or media at 37°C for 1 hour after which inoculum was removed and cells washed with acid-glycine buffer to remove loosely bound virus. Fresh media was added to all plates. The plates were incubated in a humidified 37°C incubator with 5% CO₂ for 72 hours and then harvested in western lysis buffer.

NORTHERN BLOTS

APP and tau mRNA consist of multiple splice variants. Total RNA isolated from MCMV-infected cells was subjected to northern blots as previously described.⁹⁹ Briefly, total RNA was extracted from whole cell lysates using RNazol followed by alcohol precipitation and washes and was dissolved in diethyl pyrocarbonate (DEPC) treated ultrapure water.¹⁰⁰ Total RNA was run on a 1% agarose gel containing 2% formaldehyde in RNase-free tris acetate buffer (40 mM tris, 20 mM acetic acid, 1 mM ethylenediaminetetraacetate disodium salt – EDTA). The gel was soaked in alkaline hydrolysis buffer (50 mM NaOH, 150 mM NaCl) for 30 minutes at RT and neutralized in neutralization buffer (500 mM tris, 150 mM NaCl, pH 7.5) to partially hydrolyze larger transcripts. Transfer was done onto nylon membranes using the capillary transfer method over 16 hours.

Probes were generated from plasmid pEGFP-n1-APP and tau (Addgene, Cambridge MA, #69924 and #46904 respectively). Fragments encoding the most common exons for APP were digested using HindIII and SalI restriction enzymes, fragments separated out on a 1% agarose gel, and the smaller fragment purified using Qiagen's gel purification kit (Qiagen, Cat. No. 28704) and labeled using the DIG DNA Labeling and Detection Kit (Sigma, Cat. No. 11093657910). Briefly, gel purified DNA fragments were denatured by boiling in a water bath for 10 minutes and incubated with DIG labeling reaction components overnight at 37°C. This technique was chosen over

quantitative real-time PCR because it allowed interrogation of multiple transcripts at once and for economical quantification of different splice variants.

IMMUNOFLUORESCENCE

Mouse NIH3T3 fibroblasts or primary rat cortical neurons were seeded onto 4-chambered slides at a density of 5×10^4 cells per well. After 24 hours, two wells on each slide were infected with MCMV at a MOI of 2 PFU/cell. The other two wells received an equal volume of media. Slides were kept at 37°C for an hour and then 400 μ l fresh media was added to all wells. After 24 or 48 hours, the media was removed, and cells were washed with sterile PBS twice. Cells were fixed and permeabilized by addition of ice-cold 100% methanol and incubating at -20°C for 10 minutes, after which the methanol was removed and two more washes with PBS were carried out. Blocking buffer (PBS with 5% normal goat serum) was added to all wells and slides incubated at 37°C for 30 minutes. Block buffer was replaced with primary antibody mixes (see Tables 1 and 2 for antibodies information).

Slides for fibroblasts were incubated at 37°C for 1 hour⁹⁵ and slides for neurons were incubated at 4°C overnight.⁹⁶ Following primary antibody incubation, slides were washed thrice with PBS containing 0.05% Tween-20. Appropriate secondary antibody conjugates were added to all wells and incubated at 37°C for 1 hour followed by 3 more washes with PBS-0.05% Tween-20. Chambers were removed and mounting media containing DAPI was applied. Coverslips were added and fixed by sealing edges with clear nail polish, and slides were left to cure overnight in the dark. Images were taken on

the Nikon A1R Confocal microscope at 20X or 60X objective magnification for all slides. The gain settings were set for the negative control well for each slide and the same used for image captures from the other wells for that slide.

INHIBITION OF GSK3 ACTIVITY BY LITHIUM CHLORIDE

Mouse NIH3T3 fibroblasts were plated and infected as described in the virus maintenance and infection section. After the hour of incubation with MCMV was over, the inoculum was removed, and replicate mock or infected plates received either normal media or media containing 50 mM lithium chloride (LiCl). For a third set, LiCl at 50 mM final concentration was added at 24 HPI (Figure 7). All samples were harvested at 48 HPI in western lysis buffer and subjected to total protein estimation. Western blots were performed for tau, phospho-tau S396 and phospho-tau S202 as described in the section for western blots. Conditioned media from each sample was used to titer infectious virus by standard plaque assay.

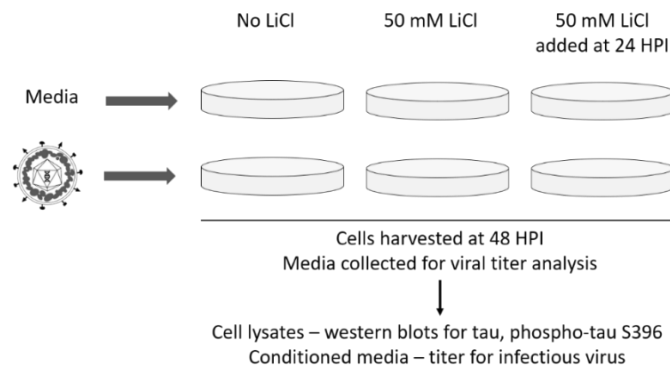


Figure 7. Experiment setup for GSK3 inhibition by lithium chloride (LiCl). Virus or media were added to plates of NIH3T3 cells for 1 hour at 37°C. Inoculum was removed and media without or with LiCl was added to respective dishes. For the third set of plates, LiCl was added at a final concentration of 50 mM at 24 HPI. All cells were harvested at 48 HPI and conditioned media collected.

STATISTICAL ANALYSES

Two-way ANOVA for repeated measures was performed followed by Fisher's least significant difference (LSD) test for comparisons of target protein levels in uninfected and infected cells. For datasets that had samples subjected to infection as well as foscarnet treatment, three-way ANOVA for repeated measures was performed followed by Fisher's LSD test. For viral titer comparison between samples in the GSK3 inhibition experiment, one-way ANOVA was performed followed by Fisher's LSD test. All statistical analyses were run in GraphPad Prism software, version 8.1. For all analyses, p-values are indicated as follows: * $p \leq 0.05$, ** $p \leq 0.001$, *** $p \leq 0.0001$, **** $p \leq 0.00001$.

CHAPTER III

RESULTS

In this project, we have analyzed whether markers involved in AD-specific neurodegeneration are altered during MCMV infection in fibroblasts comparable to the study done by Lurain et al ¹⁶, followed by a few analyses in primary rat cortical neurons. We have examined which of the three viral kinetic classes of genes are involved in alterations of amyloid and tau. We have analyzed cellular pathways of amyloid and tau and identified modifications during MCMV infection. We began by confirming that MCMV is infectious for rat neuronal cells, i.e. B35 neuroblastomas and RCN. ⁹⁴

RAT NEURONAL CELLS ARE PERMISSIVE FOR MCMV INFECTION

Demonstration of successful MCMV infection in both cell types was done by analyzing for cytopathic effect or syncytia formation, immunofluorescence and western blot detection of viral early protein 1 (E1) localized in nuclei of infected cells, and titering virus released from infected cells into media. Mouse fibroblasts were included as a control cell type, known to be fully permissive for MCMV.

When permissive cells are infected with MCMV, they often exhibit a changed morphology, i.e. rounding up, fusing together to form giant multinucleate cells as a response. This is termed syncytia formation or the cytopathic effect. ⁸³ The MCMV-infected B35 and RCN showed cytopathic effect by 24 hours post infection (HPI) similar

to that seen in MCMV-infected NIH3T3 fibroblasts (Figure 8A). Images were taken at 10X magnification.

The viral early protein E1 was detected as bright green speckles in the nuclei of infected B35 via immunofluorescence and this was similar to the speckles seen in the MCMV-infected fibroblasts (Figure 8B). When infected cells were subjected to western blotting, all four isoforms of E1 were clearly detected in B35 and RCN, like in fibroblasts (Figure 8C). From these data, we concluded that MCMV was capable of entering B35 neuroblastomas and primary RCN and starting its replication cycle.

The viral late major capsid protein (MCP) was detected as a single band of ~150 kDa in MCMV-infected rat B35 cells, like in mouse fibroblasts (Figure 8B). Thus, MCMV replication cycle could progress to late stages of infection in rat B35 neuroblastomas. The major capsid protein was below the limit of detection in MCMV-infected RCN on the western blot.

The titer obtained from MCMV-infected fibroblasts was 5×10^6 PFU/ml and was 4.3×10^6 PFU/ml for B35. This titer of infectious MCMV from the rat B35 cells taken together with expression of E1 and MCP, demonstrates that these are fully permissive for productive MCMV infection.

For the primary neurons, the titer was lower, i.e. 3×10^4 PFU/ml, which is consistent with the low amount of MCP. This was not unexpected as primary neurons are not the most permissive brain cell type for herpesvirus infection.⁸⁷ The capability of RCN to produce infectious MCMV (at a comparatively low titer) is evidence that MCMV

does undergo a complete replication cycle in these cells, even if the process may not be efficient.

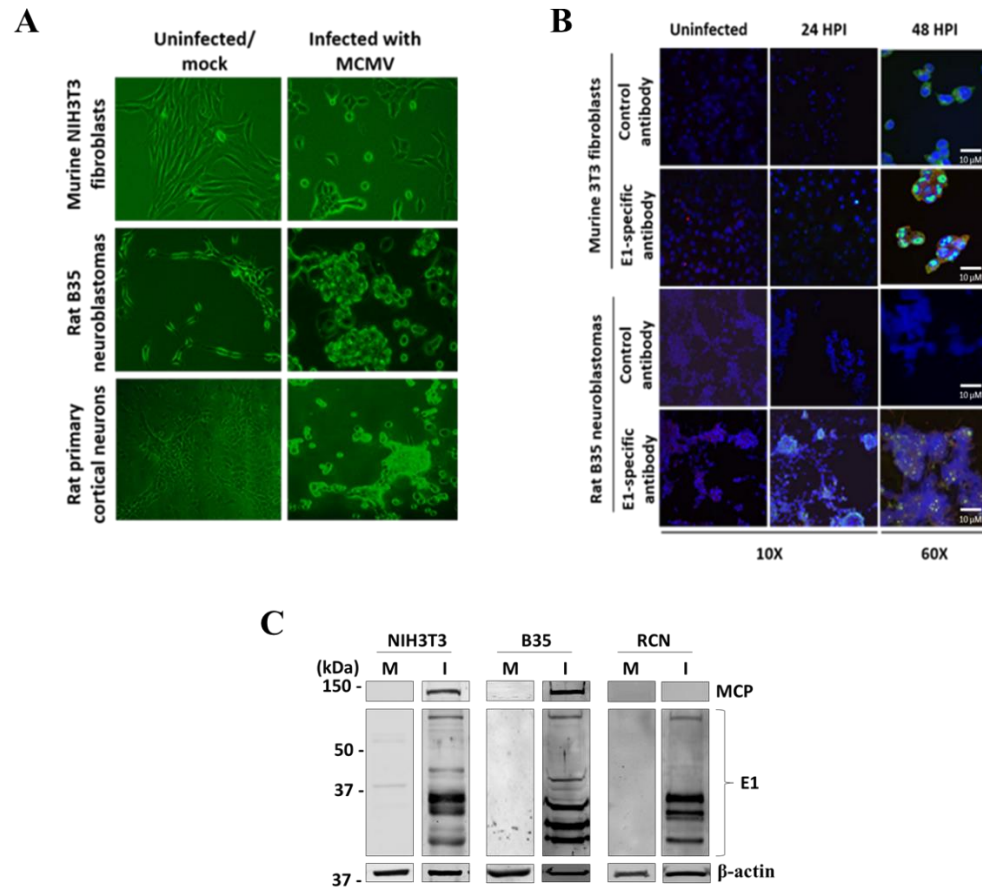


Figure 8. Rat neuronal cells are permissive for MCMV infection. (A) Syncytia formation in MCMV-infected cells at 24 HPI. Cells were infected at a MOI of 2 PFU/cell. Images were captured on a Zeiss light microscope using a 10X objective with a green filter to enhance contrast. The NIH3T3 cells were used as a control for demonstration of CMV-induced syncytia formation. (B) Immunofluorescence detection for viral early protein E1 at 24 and 48 HPI. Images were captured on Nikon A1 confocal microscope at 10X magnification for 24 HPI and at 60X magnification for 48 HPI using Nikon-Zeiss NIS Elements software. Blue staining indicates DAPI for cell nuclei. Green speckles indicate E1 detected by goat anti-rabbit FITC conjugated antibody. Pre-immune rabbit sera was used as control antibody. Polyclonal anti-E1 sera was used as the primary antibody. (C) Representative western blots showing 4 isoforms of viral early protein 1 (E1 – 62, 37, 35, and 32 kDa) and major capsid protein (MCP), a viral late protein.

EFFECTS OF MCMV INFECTION UPON THE AMYLOID PATHWAY

Results in Mouse NIH3T3 Fibroblasts

APP is Induced at Late Time Points during MCMV Infection. Lurain et al have shown increased staining of A β 42 in HCMV-infected fibroblasts.¹⁶ Other researchers have shown that HSV-1 infection increases levels of APP and A β 42.^{19,88} We hypothesized that MCMV could cause a similar increase in levels of the precursor protein like HSV-1. We therefore analyzed APP levels in mouse fibroblasts that were uninfected or infected with MCMV at MOI of 2 PFU/cell by western blotting, using rabbit polyclonal anti-APP antibody.

We successfully detected the 3 predominant APP isoforms on our western blots. Uninfected fibroblasts appear to predominantly express the 110 kDa APP isoform, with the 90 and 120 kDa ones very faintly seen on the western blot (Figure 9A left panel). Infected cells showed a significant increase in steady-state levels of APP at 48 and 72 HPI, compared to uninfected cells at the same time points (Figure 9A – 48 and 72 HPI lanes on the westerns, Figure 9B – last two data points on graph).

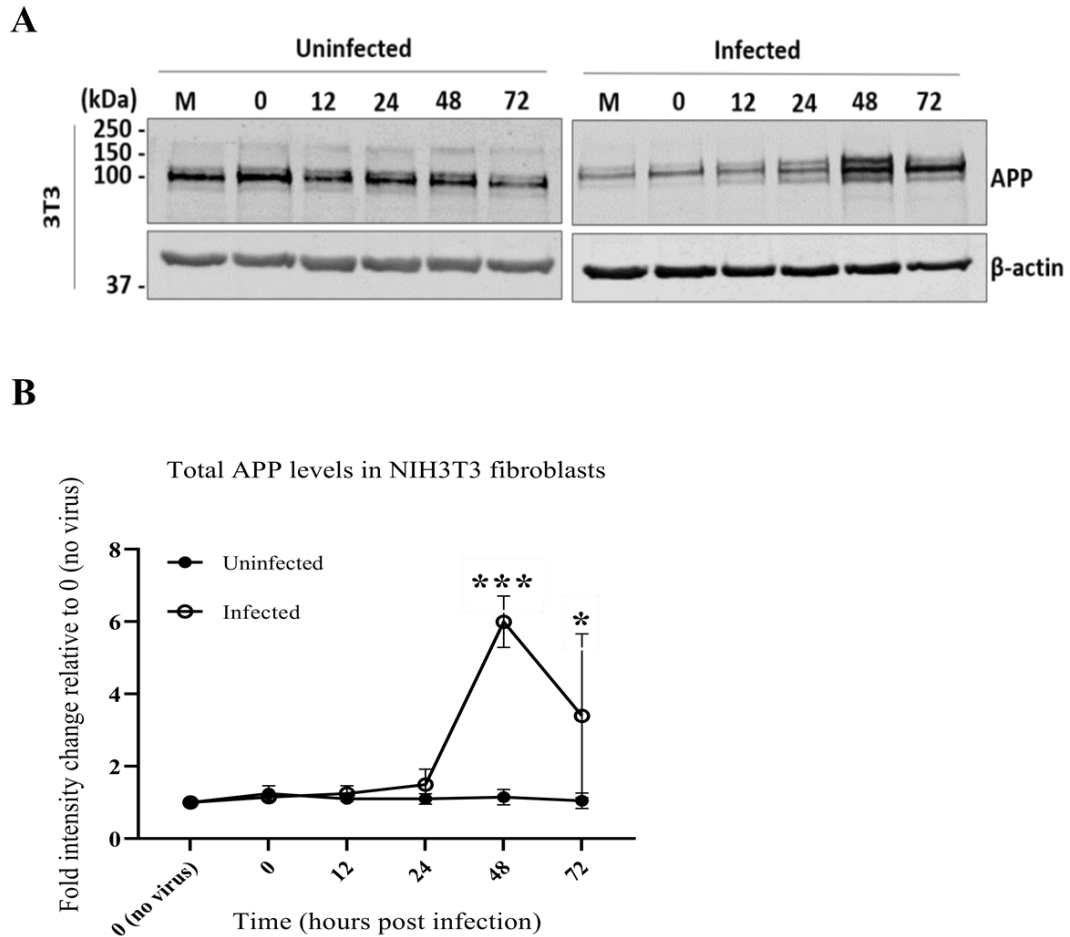


Figure 9. APP is induced during MCMV infection in mouse fibroblasts. (A) Representative western blots showing APP over 72 hours with and without MCMV infection. (B) Densitometric analyses of APP levels in uninfected and infected cells. Data were plotted as means with standard error of the mean ($n = 2$). Densitometry values were normalized for equal loading against β -actin. Level for 0 hours without virus was set as 1.0 and all time points compared to that. Two-way ANOVA for repeated measures was performed with Fisher's LSD test for multiple comparisons of APP levels between uninfected and infected cells at each time point (***) $p \leq 0.001$, * $p \leq 0.05$).

Each of the 3 APP isoforms detected (~90, 110, and 120 kDa) were then individually analyzed with scanning densitometry to investigate which of the 3 isoforms were upregulated during MCMV infection. The 120 and 90 kDa isoforms of APP were

significantly increased at 72 HPI compared to 0-no virus, 0, 12, and 24 HPI (Figure 10). The 110 kDa isoform level was not significantly different through 72 HPI compared to 0-no virus and 0 HPI. One reason for this could be the high variability between repeats of this experiment, for this dominant isoform. Western blots are semi-quantitative at best and have a multitude of factors that affect reproducibility.¹⁰¹

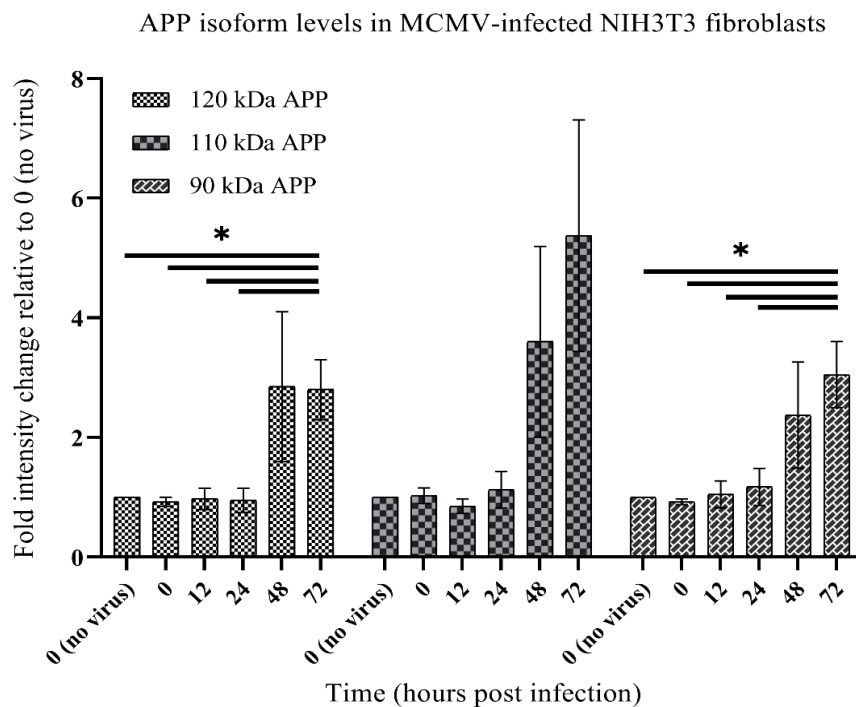


Figure 10. MCMV infection increases levels of the 90 and 120 kDa APP isoforms. For infected fibroblasts, levels of each of the 3 APP isoforms detected were quantitated, normalized against β -actin, and all time points compared to 0 hours sample without virus ($n = 4$). Two-way ANOVA for repeated measures was performed with Fisher's LSD test for multiple comparisons within each group ($*p \leq 0.05$).

Viral Late Gene Products are Involved in Altering APP Levels. The changes were seen at late time points therefore we used foscarnet (phosphonoformic acid or PFA) at a working concentration of 0.3 mg/ml volume of media, to determine if viral late gene

expression is required. Foscarnet is a current, FDA-approved antiviral; a pyrophosphate analog that inhibits the viral DNA polymerase.⁹⁸ Thus, viral genome replication is prevented, which is a necessary step for herpesviruses to express late genes.⁹⁸ Wozniak et al have shown that antivirals can reduce AD-related amyloid in cells infected with HSV-1.¹⁵ Building on this knowledge, we set up cultures of fibroblasts and tested APP levels in the presence or absence of foscarnet during MCMV infection. As the change in levels of APP was clearly evident at 48 HPI (Figure 9), we chose to focus on the effect of viral late gene inhibition at 48 HPI.

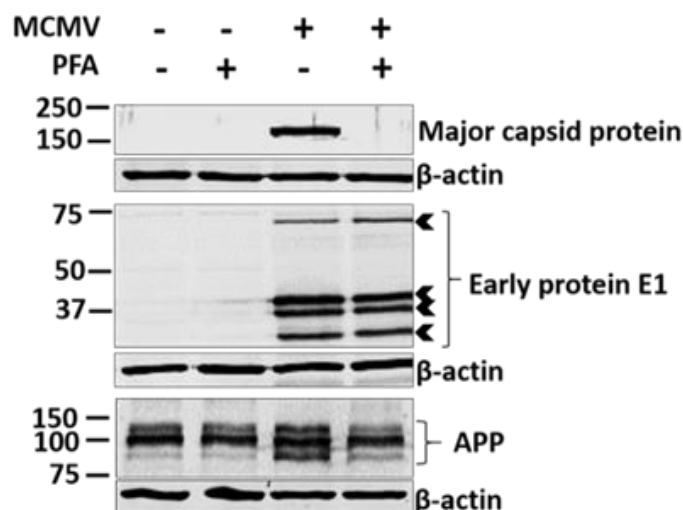


Figure 11. Viral late gene expression is necessary for induction of APP levels in fibroblasts. Mouse NIH3T3 fibroblasts were mock-infected with media or infected with MCMV (MOI 2 PFU/cell). Levels of viral proteins and APP were analyzed at 48 HPI by western blots (n = 3). Representative westerns are shown. The top panel shows viral late gene product, major capsid protein. Second panel shows the multiple isoforms of viral early protein E1. Third panel shows levels of APP. Each target protein has the matched β-actin panel beneath it to show loading. PFA – phosphonoformic acid or foscarnet.

In the absence of viral late proteins, the banding pattern for the 3 APP isoforms was similar to that from uninfected cells. The 110 kDa isoform remained unchanged in the presence of MCMV and foscarnet. However, the 90 and 120 kDa isoforms were considerably increased upon MCMV infection (Figure 11 APP panel lane 3). This increase was not seen in MCMV-infected cells that were also treated with foscarnet. Hence, we concluded that viral late proteins are involved in APP induction.

MCMV Infection does not affect Levels of Secreted A β 42. The accumulation of APP could lead to increased production of secreted A β peptides. Research has shown that secreted A β 42 and longer peptides are the ones involved in formation of plaques.^{25,29,46,47} We analyzed for amounts of secreted A β 42 peptide in media taken from uninfected and MCMV-infected fibroblasts, with or without foscarnet treatment. The sensitivity of detection by western blotting was first analyzed by using different concentrations of synthetic A β 42 peptide. The synthetic peptide was dissolved in DMEM-10% BCS media and 10-fold serial dilutions were made. These were subjected to denaturing polyacrylamide gel electrophoresis on 15-18% resolving gels followed by western blotting.

We could successfully detect concentrations ranging from 1 μ g down to 0.1 ng or 100 pg of A β 42 peptide by this method (Figure 29 in appendix). We performed western blot analysis using 60 μ l of supernatant taken from fibroblast cultures that were uninfected or infected with MCMV (MOI 2 PFU/cell) using 18% polyacrylamide gels and subjected them to western blotting. We were unable to detect A β 42 peptide in our

samples (Figure 29 in appendix). This indicated that concentrations of secreted amyloid beta peptide must be lower than 100 pg/60 μ l in our samples and a more sensitive technique was required to quantify amounts.

We then chose to quantify A β 42 levels using an ELISA with a lower limit of sensitivity of 15.6 pg/ml. As changes in APP are seen at late time points in fibroblasts, we collected media from 48 and 72 HPI fibroblasts mock-infected or infected, with or without foscarnet. We used 100 μ l of this media directly for the ELISA and were able to detect A β 42 (Figure 12). However, there was no significant difference in response to MCMV infection. All samples tested had A β 42 in the range of 200 to 250 pg/ml, which is equivalent to 12 to 15 pg in 60 μ l (Figure 12).

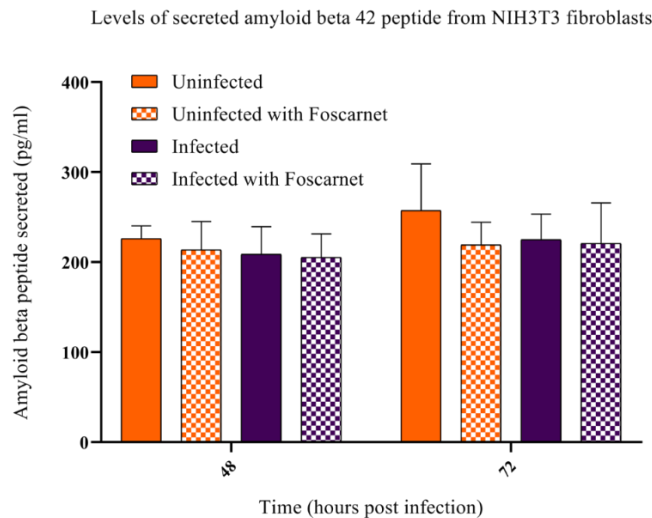


Figure 12. Levels of secreted A β 42 are not affected by MCMV infection in fibroblasts. Media from fibroblasts that were uninfected, uninfected with foscarnet, infected, and infected with foscarnet (100 μ l) was directly assayed via sandwich-based ELISA (n = 3). The OD values were normalized based on the number of cells in each sample. Data are plotted as standard error of means. Three-way ANOVA for repeated measures was performed followed by Fisher’s LSD test for multiple comparisons of each treatment with uninfected.

MCMV does not affect Levels of β and γ Secretases in Fibroblasts. APP is cleaved sequentially by β -secretase and γ -secretase (PS2) to generate 40-42 amino acid amyloid beta peptides in the amyloidogenic pathway for AD. Steady-state levels of PS2 were examined in NIH3T3 fibroblasts that were uninfected or MCMV-infected to see if these might be increased or decreased to account for APP induction and the unaltered secreted A β 42 levels.

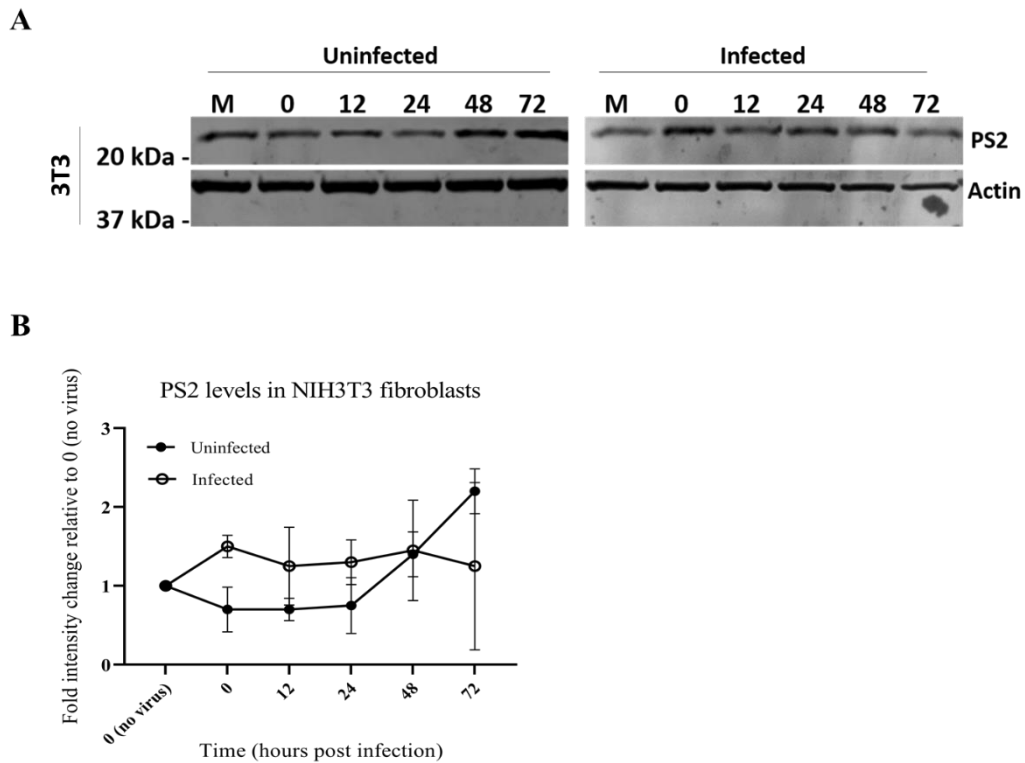


Figure 13. Levels of PS2 in fibroblasts remain unchanged with MCMV infection. (A) Representative western blot showing PS2 levels in fibroblasts infected with MCMV. (B) Densitometric analyses of PS2 levels in uninfected and infected fibroblasts. Values were normalized according to values for β -actin. Data were plotted as means with standard deviation ($n = 3$). Two-way ANOVA for repeated measures was performed with Fisher's LSD test for multiple comparisons of PS2 levels between uninfected and infected fibroblasts at each time point.

There was no statistically significant difference in the steady-state levels of PS2 in MCMV-infected fibroblasts as shown in Figure 13. From Figure 13B, it is apparent that levels increase slightly through 72 HPI in uninfected cells which was not seen for infected cells. However, these alterations are unlikely to explain the increase in APP levels.

Next, we analyzed whether the levels of β -secretase were altered in the presence of MCMV. As shown in Figure 14B, there was no significant difference in β -secretase levels in MCMV-infected fibroblasts. There was more variability in β -secretase levels in infected cells than in mock-infected cells, and this may explain why the difference in β -secretase levels at 48 and 72 HPI is not statistically significant.

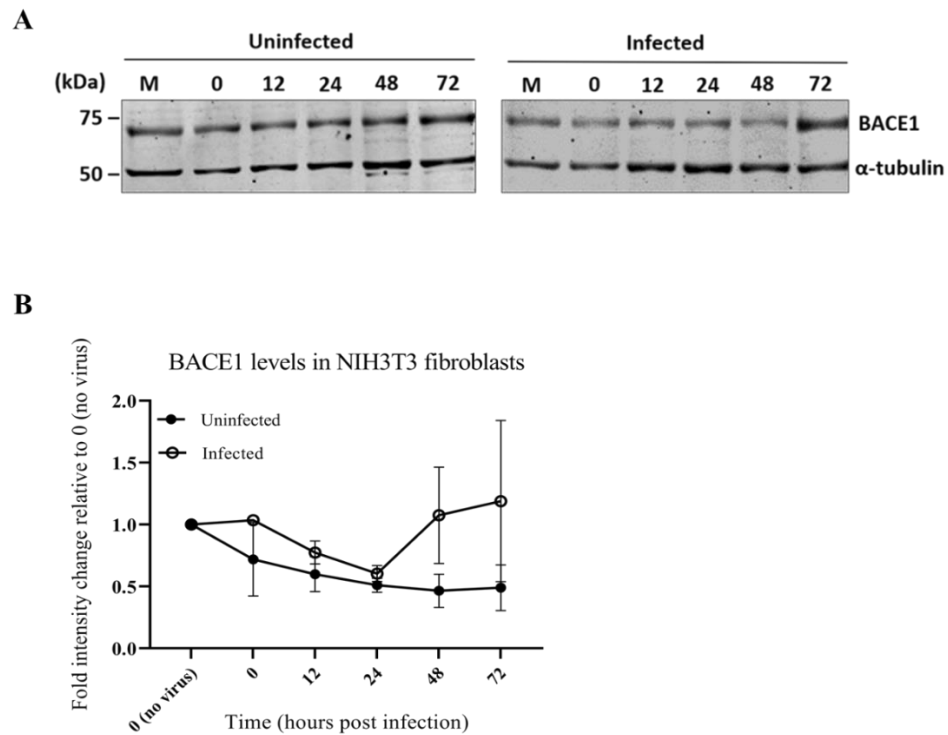


Figure 14. Analyses of β -secretase levels in NIH3T3 fibroblasts during MCMV infection. (A) Representative western blots showing β -secretase protein in uninfected and infected fibroblasts. (B) Densitometric analysis of β -secretase levels ($n = 3$). Values were normalized according to values for β -actin. Data are plotted as standard error of means. Two-way ANOVA for repeated measures was performed followed by Fisher's LSD test for multiple comparisons of uninfected and infected samples at each time point.

Activity of β -secretase is Upregulated during MCMV Infection. The activity of β -secretase was then assessed by a fluorometric assay based on principles of ELISA (Figure 15). The activity of β -secretase was significantly decreased in infected cells with and without foscarnet as compared to uninfected at 72 HPI. However, the results are more reflective of an increase in β -secretase activity in uninfected fibroblasts at 72 HPI and when this is used for comparison, a decrease in the MCMV-infected cells is seen at 72 HPI. Over time, the uninfected cells may be inducing β -secretase activity as part of their normal metabolism and hence, it is difficult to say conclusively that MCMV infection reduces β -secretase activity.

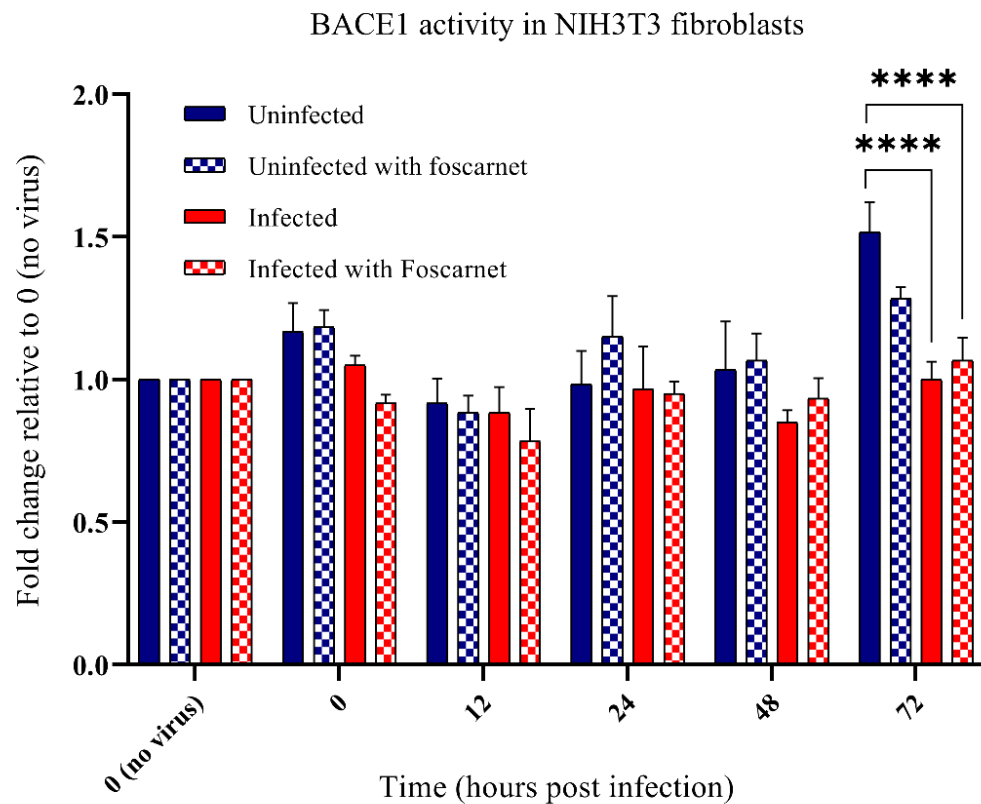


Figure 15. Activity of β -secretase is reduced in MCMV-infected fibroblasts. Fold changes in β -secretase activity during MCMV infection with and without foscarnet. Activity was measured using a fluorometric assay ($n = 2$). Values were normalized according to total protein in cell lysates. Data are plotted as standard error of means. Three-way ANOVA for repeated measures was performed followed by Fisher's LSD test for multiple comparisons of each treatment with uninfected (PFA – foscarnet, **** $p \leq 0.00001$).

Thus, MCMV infection in mouse NIH3T3 fibroblasts, causes an induction of APP and viral late proteins are involved. The levels of secreted A β 42 peptide, γ -secretase (PS2), and β -secretase remain unchanged. However, the activity of β -secretase was not increased at 72 HPI in MCMV-infected cells as it was in uninfected cells.

Results in Rat Neuronal Cells

Levels of APP in Rat Primary Cortical Neurons (RCN). We tested levels of APP, levels of secreted A β 42, APP mRNA, and levels of γ -secretase in primary RCN that were uninfected or infected with MCMV. The levels for APP in primary rat cortical neurons showed no statistically significant changes as shown in Figure 16. The levels were not increased in infected cells as compared to uninfected (Figure 16A). The levels of all 3 APP isoforms did not vary through 72 HPI in infected cells (Figure 16B), and this was different from what was obtained in MCMV-infected fibroblasts.

To address whether this was due to cells being of neuronal lineage and untransformed, we tested APP levels in rat B35 neuroblastomas (Figure 29 in appendix). The results for both types of rat neuronal cells were similar and neither showed APP increase, unlike fibroblasts. Thus, we suggest that MCMV effects on APP may be cell-type specific, however, it could also be species-specific as both the RCN and B35 are rat cells.

We analyzed conditioned media from the same uninfected and infected RCN using an ELISA kit specific for rat secreted A β 42 with sensitivity down to 6.25 pg/ml. All sample readings were lower than those detected for the control wells. Control wells had fresh media added to them (sterile, had never been in contact with cells). These control readings were comparable to 60 pg/ml and all sample readings were lower than those. Hence, we inferred that the neurobasal media with B27 and glutamine supplement might be interfering with detection of the peptide in samples from rat primary neurons.

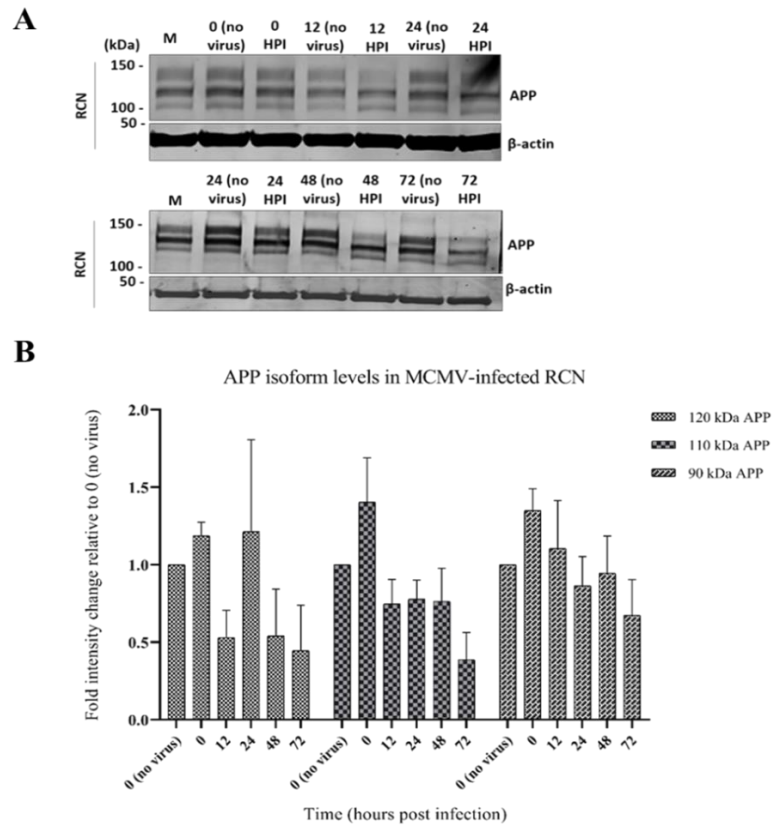


Figure 16. MCMV infection in primary rat cortical neurons does not induce changes in APP levels. (A) Representative western blots showing APP over 72 hours with and without MCMV infection ($n = 2$) using rabbit anti-APP primary antibody. (B) For infected cells, levels of each of the 3 APP isoforms detected were quantitated with scanning densitometry, normalized against β -actin, and all time points compared to 0 hours without virus. Two-way ANOVA with uncorrected Fisher's LSD test was performed.

Thus, in primary RCN, APP is not induced during MCMV infection. This effect may be because these are neuronal. This is more likely since NIH3T3 fibroblasts and B35 neuroblastomas are both transformed cell lines and there was no difference in APP levels in the B35 cells, like the primary neurons. There may be more efficient processing of APP in neurons. Analyses of $A\beta_{42}$ would help answer whether this is the case for APP.

Examination of β -secretase and γ -secretase levels and activity would validate whether MCMV infection can be used as an experimental system in animal models of AD.

EFFECTS OF MCMV INFECTION UPON TAU AND ITS PHOSPHORYLATION

Results in Mouse NIH3T3 Fibroblasts

MCMV Infection Upregulates Total Tau. Researchers have shown that HSV-1 infection is capable of upregulating total tau levels and phosphorylation.^{14,15} We were unable to find published literature regarding CMV infection and tau protein levels or their modifications specific to AD. We analyzed whether MCMV can affect tau levels or modifications. Tau is expressed as six protein isoforms translated from splice variants.⁵² The six isoforms range in size from 35 to 46 kDa without post-translational modifications. There are also smaller cleaved tau products with varying functions in the cells and extensive posttranslational modifications.⁵⁵ Thus, tau forms can range from 25 to 200 kDa in size.

We found that CMV infection induces levels of total tau in infected cells and the banding patterns for tau forms were different compared to uninfected cells (Figure 17A). From 12 to 72 HPI, the intensity of the dark tau band (~80 kDa) decreased whereas bands above 100 kDa and in the range of 50-70 kDa became apparent. A few of the faster migrating tau forms were stabilized till 24 HPI before disappearing whereas the same sized forms in uninfected cells disappeared starting at 12 HPI. For the densitometry (Figure 17B), intensities of all tau bands in each lane were added and then fold change was calculated relative to tau in the 0-no virus lane.

An additional comparison was done by grouping tau band intensities from 50-250 kDa (high molecular weight tau with likely posttranslational modifications) and from 25-50 kDa (low molecular weight unmodified tau and cleavage products), to show that the increase in overall tau was primarily due to increased high molecular weight tau bands (Figure 17C).

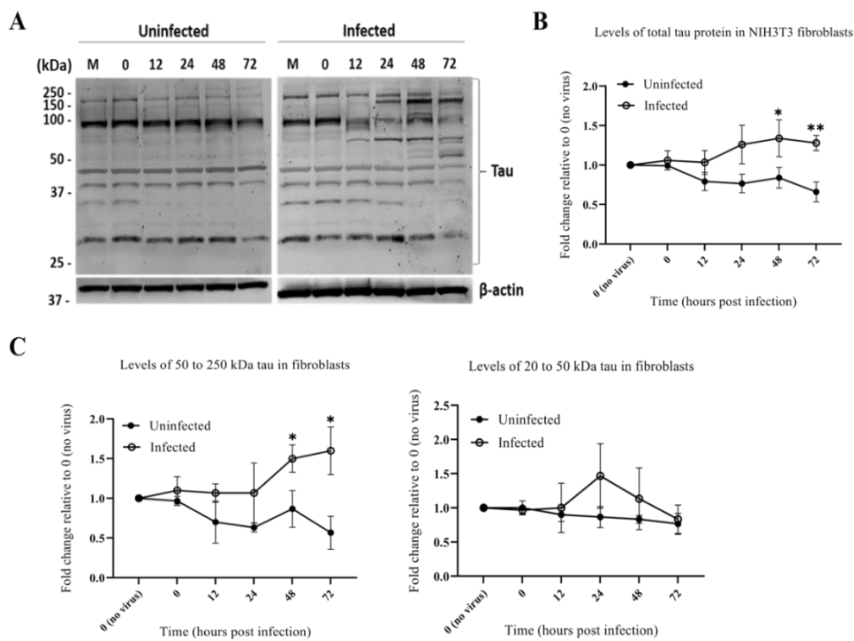


Figure 17. Total tau is induced upon MCMV infection in fibroblasts. (A) Representative western blots showing total tau over 72 hours with and without MCMV infection. (B) Scanning densitometry analyses of tau levels in uninfected and infected cells. Data were plotted as means with standard deviation ($n = 3$). Densitometry values were normalized for equal loading against β -actin. Level for 0 hours without virus was set as 1.0 and all time points compared to this. Two-way ANOVA for repeated measures was performed with Fisher's LSD test for multiple comparisons of tau levels between uninfected and infected cells at each time point (** $p \leq 0.001$, * $p \leq 0.05$). (C) Densitometric analysis was done as in B except band intensities were grouped by molecular weight ranges 50-250 kDa and 20-50 kDa.

Viral Late Genes are Required for Tau Increase. The levels of total tau were increased at late time points, so we used foscarnet to inhibit viral late gene products in fibroblasts to determine whether late gene expression was required, or this was just a slow response. Representative western blots confirming successful inhibition with foscarnet are shown in Figure 18. Levels of β -actin were unchanged in the presence of MCMV and/or foscarnet. Viral early protein m143 was expressed in MCMV-infected cells in the presence/absence of foscarnet. Major capsid protein (MCP – viral late protein) was only expressed in MCMV-infected fibroblasts without foscarnet treatment. These controls show that infection and treatment worked as expected.

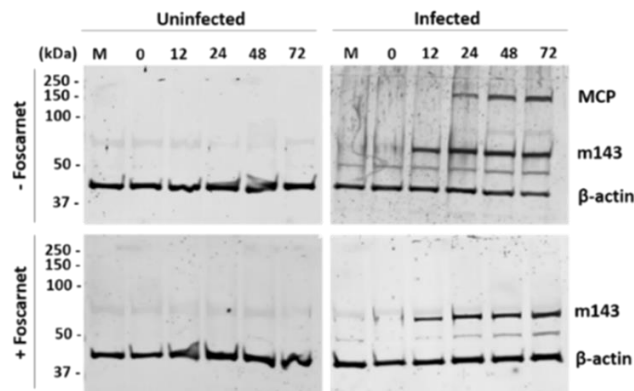


Figure 18. Representative western blots for demonstration of successful MCMV infection and foscarnet treatment. MCP – major capsid protein: a viral late protein, m143 – viral early protein.

Figure 19 shows 4 representative western blots for total tau. There were no changes to total tau banding patterns for uninfected cells treated with foscarnet (Figure 19A left-hand side top and bottom blots). With foscarnet treatment of infected cells, the intensities for bands of high molecular weight tau were reduced at 72 HPI (Figure 19B).

A significant increase in tau bands of 70-250 kDa size was detected at 48 and 72 HPI in the absence of foscarnet. From this result, we concluded that viral genome replication and late gene products are involved in induction of tau levels. Figure 19B shows the densitometric analysis for total tau westerns. Since predominant tau band changes were in the 50-250 kDa range, densitometric analyses for the same are shown in Figure 19B.

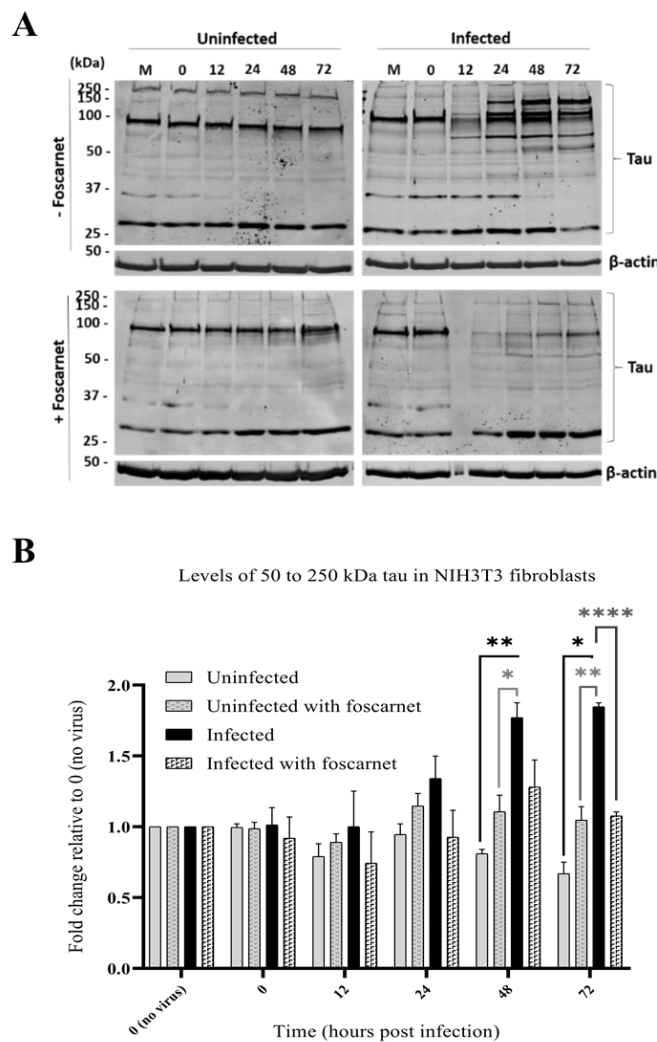


Figure 19. Viral late gene expression is necessary for tau induction. (A) Representative western blots showing total tau during infection with or without viral late gene inhibition (foscarnet

treatment). (B) Scanning densitometry analyses of 50-250 kDa tau in cells treated with foscarnet or virus or both compared to uninfected-untreated. Data were plotted as means with standard deviation ($n = 3$). Densitometry values were normalized for equal loading against β -actin. Level for 0 hours without virus was set as 1.0 and all time points compared to this. Two-way ANOVA for repeated measures was performed with Fisher's LSD test for multiple comparisons of tau levels between uninfected and infected cells at each time point ($*p \leq 0.05$, $**p \leq 0.001$, $****p \leq 0.00001$).

Tau Induction is not a Cellular Response to Virus Entry/Virion Components.

To confirm that tau induction was mediated by MCMV and was not partly due to a delayed cellular response to virus entry, we used wild-type (WT) and UV-inactivated virus for infecting fibroblasts and analyzed tau levels at 72 HPI. Both viruses are capable of binding and entering cells at 37°C; however, only the WT virus undergoes productive infection (Figure 6A in Chapter 2). We found that productive virus infection is required for causing the upregulation of total tau proteins (Figure 20). The levels of tau in cells infected with the UV-inactivated virus remained the same as those in uninfected cells (Figure 20A). Thus, viral binding, entry and the presence of virion components were not sufficient for causing tau induction. Figure 20B shows the viral markers for experiment controls. The four isoforms of E1 are detectable at a low level in cells infected with UV-inactivated MCMV. This was due to the presence of very few infectious virus particles that were not UV-inactivated (titer 50 PFU/ml).

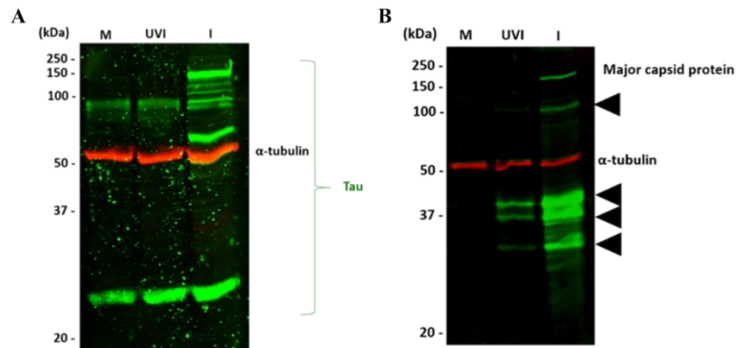


Figure 20. Viral binding and entry is not sufficient to induce total tau levels in fibroblasts. (A) Western blot showing tau levels in fibroblasts during different conditions at 72 HPI. UVI – UV-inactivated MCMV, M – mock, I – infected. (B) Representative western blots (n = 2) showing expression of viral early and late proteins for demonstration of experiment conditions at 72 HPI. MCP – major capsid protein. Filled triangles indicate the 4 isoforms of viral early protein 1 (E1).

Infection with MCMV changes the tau banding pattern compared to uninfected cells. Given the size range of enhanced bands (70 – 250 kDa) well above the range of 35-46 kDa range of unmodified tau, this is suggestive of changes happening in post translational modifications of tau isoforms during MCMV infection. Hence, we analyzed tau phosphorylation at two sites (S396 and S202) known to be increased in AD^{52,102} and also shown to be affected during HSV-1 infection.¹⁴ Induction of phosphorylation at these 2 sites during HSV-1 infection was shown in human neuroblastoma cells, however this was studied only at 16 HPI via immunofluorescence, so sizing and quantitation is lacking.¹⁰³

Tau Phosphorylation at Serine 396 is Increased during MCMV Infection.

Uninfected fibroblasts have little phosphorylation at S396 as shown in Figure 20A. Upon MCMV infection, there was a significant induction of tau phosphorylation at S396

starting at 24 HPI and increasing through 72 HPI (Figure 21). The enhanced phosphorylation at S396 was seen as intense bands high in molecular weight. Therefore, we focused our densitometric analysis on phosphorylated tau forms that were 50 to 250 kDa in size (Figure 20B) on our western blots. The size ranges of these modified tau bands are similar to those seen for total tau (100-250 kDa) in Figure 16, for infected fibroblasts. Hence, MCMV infection induces tau phosphorylation at S396 as well as total tau. Both these changes have been documented for AD as being important for the formation of neurofibrillary tau tangles.¹⁰⁴

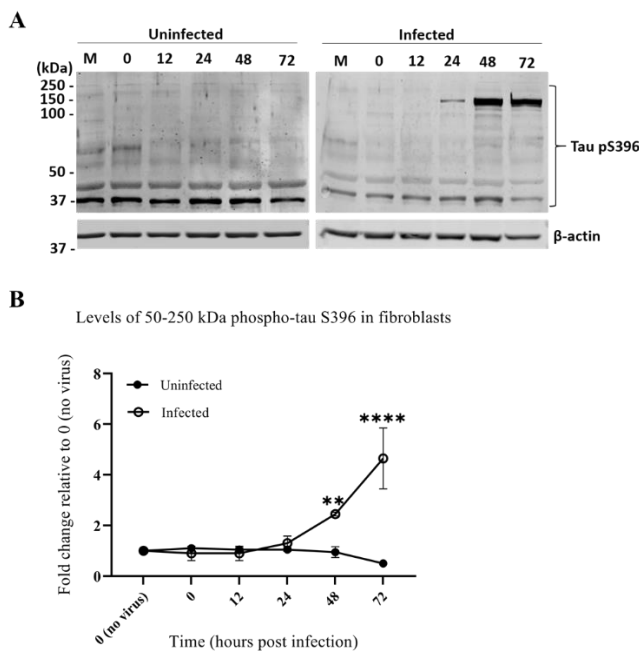


Figure 21. Phosphorylation of tau at serine 396 is induced at late times during CMV infection. (A) Representative western blots showing tau phosphorylated at serine 396 over 72 hours with and without MCMV infection. (B) Densitometric analyses of phosphorylation at S396 levels in uninfected and infected cells. Data were plotted as means with standard deviation (n = 3). Densitometry values were normalized for equal loading against β -actin. Level for 0 hours without virus was set as 1.0 and all time points compared to that. Two-way ANOVA for repeated

measures was performed with Fisher's LSD test for multiple comparisons of tau levels between uninfected and infected cells at each time point (** $p \leq 0.001$, **** $p \leq 0.00001$).

Tau phosphorylation at S396 was induced starting at 24 HPI through 72 HPI, so we inhibited viral late gene expression by using foscarnet.⁹⁸ In the absence of viral late proteins, there was no evidence of phosphorylation at S396 for tau (Figure 22A bottom right blot) compared to uninfected cells (Figure 22 top left blot). Foscarnet treatment did not affect tau phosphorylation at S396 in uninfected cells (Figure 22A left-hand side top and bottom blots).

Figure 22B shows the densitometric analysis of western blots represented in Figure 22A. The prevention of increase of tau phosphorylation at S396 was significant for 24 and 72 HPI. The same reduction is apparent from the western blots and the graph at 48 HPI also, however, it was not statistically significant. This may be due to the high variability within the western blotting process between the experiment repetitions. Thus, CMV infection induces phosphorylation at S396 and viral late gene expression is required for this induction. The viral immediate-early or early gene products do not seem to be involved in inducing this particular tau modification.

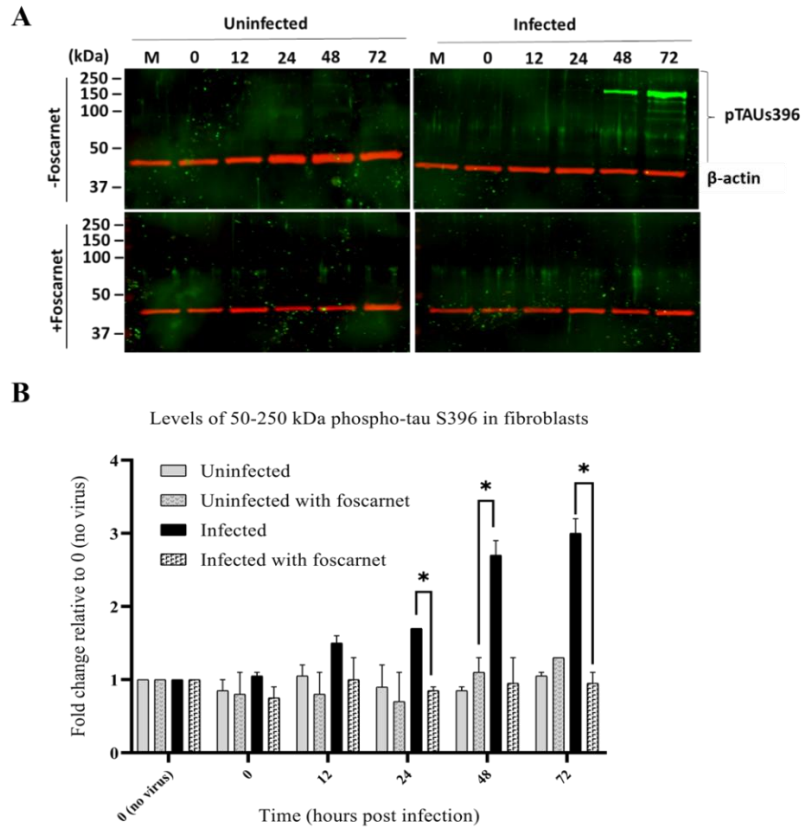


Figure 22. Viral late gene products are required for induced phosphorylation of tau at S396, in fibroblasts. (A) Representative western blots showing tau phosphorylated at S396 in uninfected or infected fibroblasts, with or without foscarnet treatment. (B) Scanning densitometry analyses of 50-250 kDa phospho-tau (S396) in cells treated with foscarnet or virus or both compared to uninfected-untreated. Data were plotted as means with standard deviation ($n = 3$). Densitometry values were normalized for equal loading against β -actin. Level for 0 hours without virus was set as 1.0 and all time points compared to this. Two-way ANOVA for repeated measures was performed with Fisher's LSD test for multiple comparisons of tau levels between uninfected and infected cells at each time point ($*p \leq 0.05$).

Tau Phosphorylation at S202 remains Unchanged through MCMV Infection.

Considering that serine 202 was another site shown to be increasingly phosphorylated during HSV-1 infection¹⁴, we analyzed whether the same was true for MCMV. In fibroblasts, there was no difference seen in banding patterns for phosphorylation at serine

202 in MCMV-infected cells (Figure 22). Uninfected fibroblasts had more phosphorylation at S202 than what was detected for S396 (Figures 20 and 22). While the phosphorylation at S396 was induced after MCMV infection, no significant change was detected for tau phosphorylation at S202 (Figure 22A). Thus, we concluded that MCMV infection induces site-specific modifications on tau.

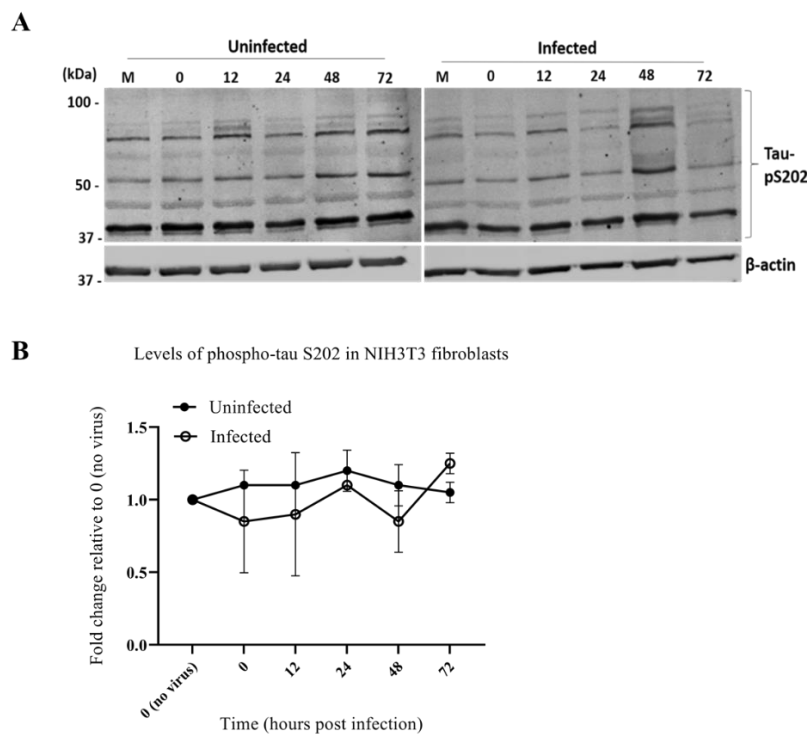


Figure 23. MCMV infection does not affect phosphorylation of tau at serine 202 in fibroblasts. (A) Representative western blots showing tau phosphorylated at serine 202 over 72 hours with and without MCMV infection in NIH3T3 fibroblasts. (B) Scanning densitometry analyses of the same in uninfected and infected fibroblasts. Data were plotted as means with standard deviation ($n = 2$). Densitometry values were normalized for equal loading against β -actin. Level for 0 hours without virus was set as 1.0 and all time points compared to that. Two-way ANOVA for repeated measures was performed with Fisher's LSD test for multiple comparisons of tau levels between uninfected and infected cells at each time point.

Results in Primary RCN

MCMV Infection affects Tau in a Manner Similar to that Seen for

Fibroblasts. Since amyloid and tau are neurodegenerative disease markers, testing effects that MCMV infection has in a relevant cell type is important. When we analyzed MCMV-infected primary RCN for alterations of markers in the amyloid pathway, we found that there were differences in the patterns seen between mouse fibroblasts and rat neurons. We tested whether the same was true for tau proteins in MCMV-infected neurons compared to fibroblasts. The following data presented are preliminary results.

We found that total tau was induced with banding patterns similar to those seen for fibroblasts, for primary RCN (Figure 24A). There was an increase in the number of bands for tau as well as enhancement of slower migrating forms in the size range of 70 to 250 kDa, compared to uninfected neurons. Tau phosphorylation at S396 was detected as 4 predominant bands ranging from ~65 to 100 kDa uninfected cells (Figure 24B). With the progress of MCMV infection, high molecular weight forms became apparent starting at 24 HPI through 72 HPI in the range of 100-250 kDa, like those seen for fibroblasts. Both these results for total tau and phospho-tau S396 confirmed that MCMV has similar effects on tau in mouse fibroblasts and rat neurons.

We then tested for levels of tau phosphorylated at S202. Due to the reduced availability of the primary cells, we only analyzed one early and one late time point (12 and 48 HPI). At both these times, there was no difference in phosphorylation at S202 between the uninfected and MCMV-infected primary neurons. This result further

confirmed that MCMV affects tau and its above-mentioned modifications similarly via a possibly conserved mechanism.

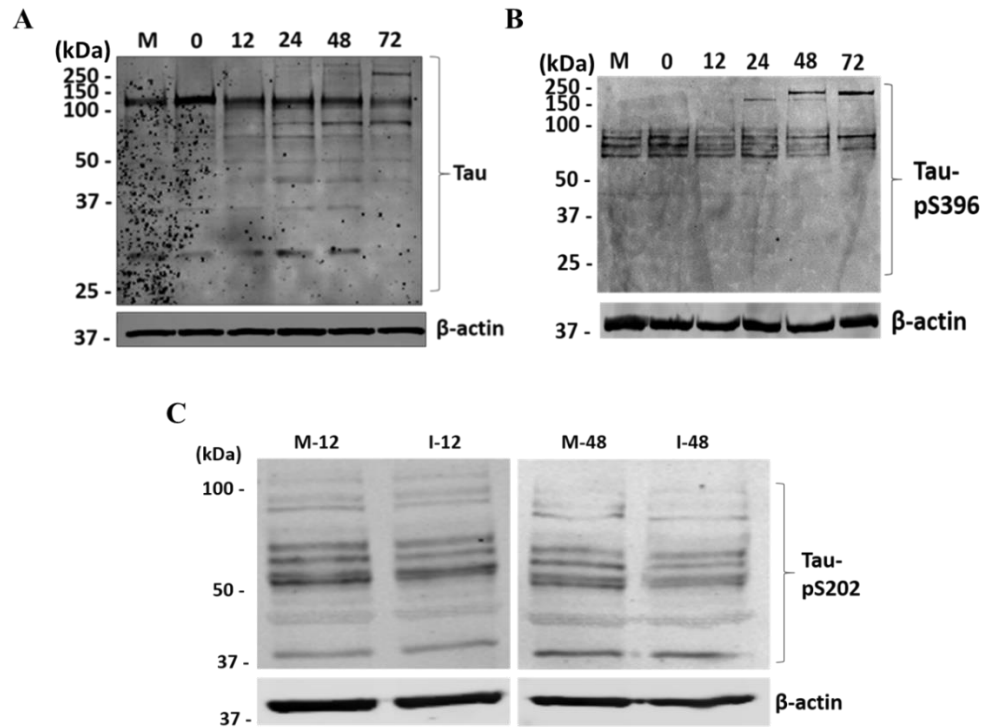


Figure 24. Tau and its phosphorylation at S396 and S202 is affected in a similar manner in primary RCN. (A) Western blot showing total tau in MCMV-infected RCN over 72 HPI. (B) Western blot showing tau phosphorylated at S396 in MCMV-infected RCN over 72 HPI. (C) Western blots showing tau phosphorylated at S202 in uninfected and infected RCN at 12 and 48 HPI. Loading control for all blots was β -actin.

Since the alterations in primary neurons were like those seen for NIH3T3 fibroblasts, we suggest that fibroblasts can be useful as a model to perform further experiments for elucidating mechanisms of how MCMV alters tau and its modifications. We also examined the banding patterns of total tau and phospho-tau (S396 and S202) in rat B35 neuroblastomas (Figures 33 and 34 in appendix). We found that the enhancement

of high molecular weight tau forms (total and S396) was increased similar to that seen in MCMV-infected mouse fibroblasts and rat neurons.

The cellular kinase called GSK3 β is implicated in AD tau pathology^{61,105} as well as upregulated during HSV-1 infection.¹⁴ Both the sites of phosphorylation examined (S396 and S202) can be phosphorylated by GSK3 β , along with many other kinases.^{60,61} However, S396 is phosphorylated by a greater number of kinases than S202.^{59,61,106} Since we saw no changes in phosphorylation of tau at S202 but dramatic changes at S396, this reduced the likelihood of GSK3 being involved with upregulation of tau phosphorylation by MCMV but did not completely rule it out. MCMV could be mediating tau phosphorylation at S396 in a kinase dose-dependent or time-dependent manner.

MCMV Infection and Effects on GSK3 in NIH3T3 Fibroblasts. CMV is known to incorporate host phosphatases in its virion and upregulate host phosphatases upon infection.¹⁰⁷ Given the enhancement of slower migrating forms of phosphorylated tau (S396) in MCMV-infected cells (Figure 21), it is highly likely that kinases play a role. We tested whether there was an induction of GSK3 β protein levels during MCMV infection in NIH3T3 fibroblasts and found that over 72 HPI, there was no significant change in GSK3 β levels (Figure 25A and B).

The increased phosphorylation of tau at serine 396 taken together with no change in phosphorylation at serine 202 and no change in GSK3 β levels suggests that either CMV does not induce phosphorylation via GSK3 β or it modulates the activity of this

enzyme. Lithium chloride can inhibit GSK3 and prevent phosphorylation of its target proteins.¹⁰⁸ We inhibited GSK3 using 50 mM lithium chloride and analyzed levels of total tau and tau phosphorylation at S396. In this case, if GSK3 were important for sites other than S396, we should detect changes in the sizes of shifted bands.

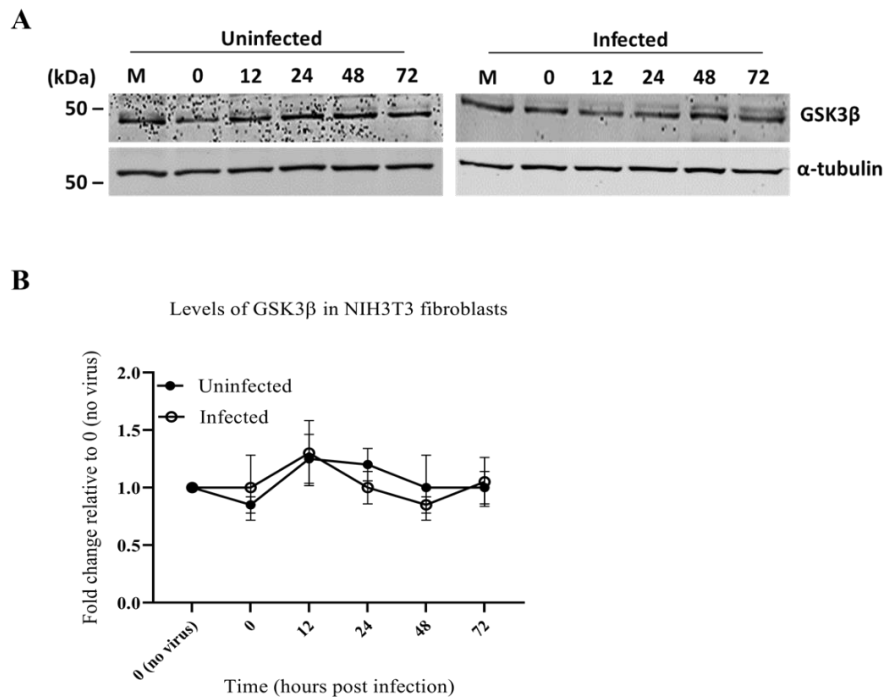


Figure 25. MCMV infection does not affect levels of GSK3β in fibroblasts. (A) Representative western blots showing levels of GSK3β in uninfected and infected cells. (B) Densitometric analysis for GSK3β levels in uninfected and infected fibroblasts. Data are plotted as means with standard deviation (n = 3). Densitometry values were normalized for equal loading against β-actin. Level for 0 hours without virus was set as 1.0 and all time points compared to that. Two-way ANOVA for repeated measures was performed with Fisher's LSD test for multiple comparisons of GSK3β levels between uninfected and infected cells at each time point.

In our GSK3 inhibition experiments, we also included samples where uninfected and infected cells were given LiCl 24 HPI. Since the phosphorylation at S396 was highly

increased between 24 and 48 HPI, if GSK3 was involved, we would expect the tau band pattern to be similar in both sets of infected cells (with LiCl added at 24 HPI and at 0 HPI). This was set up to examine whether belated addition of LiCl was sufficient to reverse GSK3-mediated total tau and tau phosphorylation (S396) increase. In previous studies, it has been shown that addition of a similar salt, NaCl, does not inhibit GSK3. This effect is specific to LiCl.¹⁰⁹

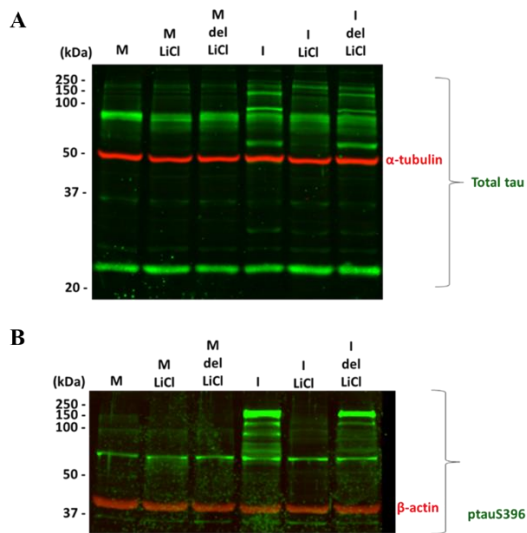


Figure 26. Inhibition of GSK3 from onset of MCMV infection has very little effect on total tau and phospho-tau S396. (A) Western blot showing total tau in uninfected and MCMV-infected fibroblasts at 48 HPI with different treatments. (B) Western blot showing tau phosphorylated at S396 in uninfected and MCMV-infected fibroblasts at 48 HPI with different treatments. Loading controls used were α -tubulin and β -actin. M – mock/uninfected, I – infected, M-LiCl – uninfected cells treated with 50 mM LiCl throughout 48 HPI, I-LiCl – infected cells treated with 50 mM LiCl throughout 48 HPI, M del LiCl – uninfected cells with LiCl added at 24 HPI, I del LiCl – infected cells with LiCl added at 24 HPI.

We found that LiCl treatment for 24 or 48 hours did not alter tau or its phosphorylation at S396 in uninfected cells (first 3 lanes of blots shown in Figure 26A and B). Treatment with LiCl kept throughout 48 hours, prevented the induction of tau

and tau phosphorylation at S396 (Figure 26 lane labeled I-LiCl on western blots shown in A and B). The banding pattern looked similar to uninfected cells. With belated addition of LiCl at 24 HPI, there were only small differences in the banding patterns for total tau and tau phosphorylation at S396 (Figure 26 last lane on blots labeled I del LiCl). For total tau, the relative intensities of some of the intermediate sized bands appeared reduced. This was consistent with the S396 with the slowest migrating tau form (150-250 kDa) still being abundant but the smaller bands (50-100 kDa) being less intense. No new bands appeared.

There is published evidence for LiCl being inhibitory to HSV-1.¹⁰⁹⁻¹¹¹ We tested whether viral early and late proteins or production of infectious virus was affected by the addition of lithium chloride. When LiCl was present throughout, early protein m143 was produced at a barely detectable level and the late protein, major capsid protein (MCP), was below the limit of detection (Figure 27A, right-hand blot lane labeled I LiCl). Belated addition of LiCl did not lead to a reduction in either viral marker (Figure 27A last lane on right-hand blot). The infectious virus titer was reduced by 5-logs when LiCl was present throughout infection whereas it was only different by 1-log when LiCl was added at 24 HPI (Figure 27B). So, LiCl is capable of severely inhibiting MCMV.

Thus, the lack of changes in total tau and phosphorylation of tau at S396, in the cells treated with LiCl throughout infection, is likely due to a lack of induction of GSK3. However, since viral late genes were expressed normally with the delayed addition of the LiCl, we can see that GSK3 inhibition has minimal effect on either total tau banding

pattern or phosphorylated tau (S396). Hence, other kinases are likely more important in the context of MCMV infection.

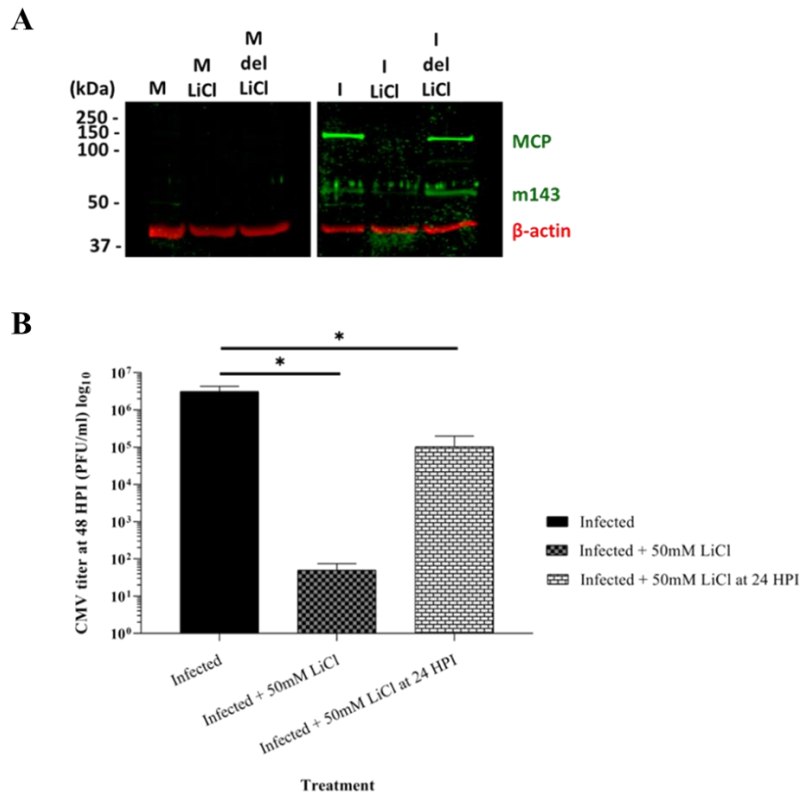


Figure 27. MCMV is inhibited by LiCl. (A) Representative western blots showing expression of viral early and late proteins in presence or absence of LiCl or delayed addition. (B) Graph showing titer of infectious virus released at 48 HPI from MCMV-infected cells with LiCl treatment throughout and for the last 24 hours. Data are plotted as means with standard deviation ($n = 3$). Ordinary one-way ANOVA was performed followed by Fisher's LSD test for multiple comparisons. Values were compared to infected sample without any treatment ($*p \leq 0.05$).

CHAPTER IV

DISCUSSION

Based on the data presented, we propose the model shown in Figure 28 for interactions of mouse CMV with amyloid and tau pathways. Viral late gene products are involved in inducing APP, tau and tau phosphorylation at S396. There is no increase in the activity of β -secretase late during MCMV infection. Kinases other than GSK3 are involved in increased tau phosphorylation at S396.

While the results for amyloid markers are different in the primary RCN and B35 cells from fibroblasts, MCMV has similar effects on tau and its modifications in neuronal cells. This is promising for future *in vivo* studies on tau in animal models of neurodegenerative diseases and for examining relative importance of dysfunctional tau in some amyloid transgenic animal models.

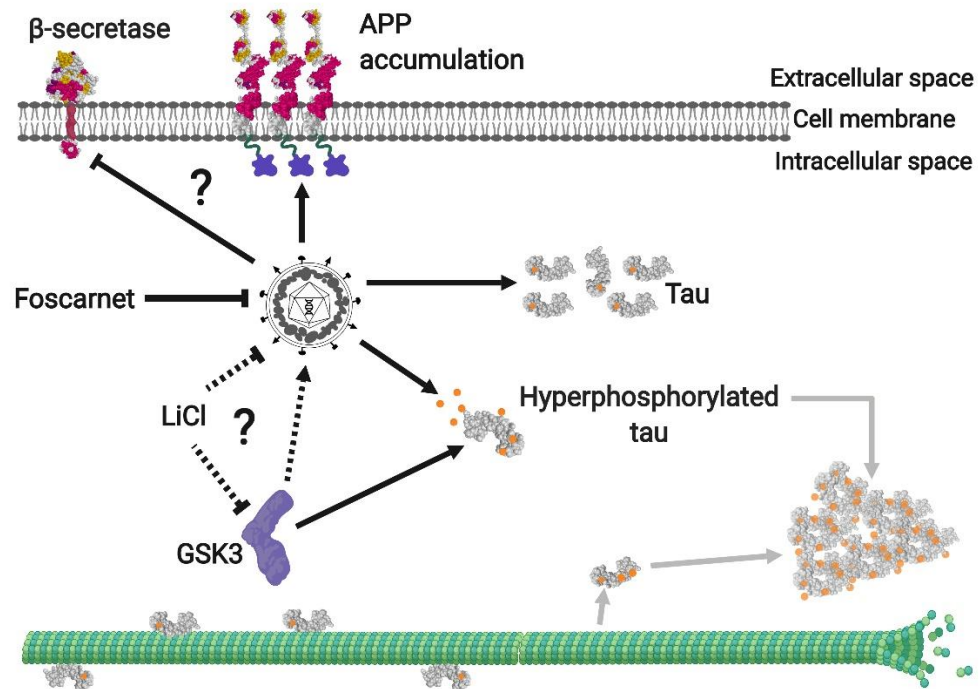


Figure 28. Proposed model of MCMV interactions with amyloid and tau pathways of neurodegeneration. MCMV upregulates APP, tau, and hyperphosphorylated tau. Inhibition of viral replication with foscarnet abolishes these increases. The activity of β -secretase is not increased during MCMV infection. Lithium chloride inhibits GSK3 and MCMV. Black arrows – leads to, black inhibitor arrows – inhibits. Dashed arrow and dashed inhibitor lines – potential pathways. Gray arrows show that abnormally phosphorylated tau detaches from microtubules and forms aggregates in AD.

MCMV AND AMYLOID

There is published literature on HSV-1 interactions with APP^{19,20,88} and HCMV's correlation with increased A β 42¹⁶ in tissue culture. Cheng et al have shown that outgoing, newly formed HSV-1 particles directly interact with APP while egressing in vesicles along microtubules.¹⁹ We have shown that MCMV late gene products are involved in upregulating steady-state levels of APP in fibroblasts (Figure 9). However,

APP levels remain unchanged in rat neuronal cells (Figure 29 in appendix and Figure 16) despite evidence for CMV infecting various cell types in rodent brain.¹¹² This could be because CMV interacts differently with cellular proteins in different cell types or may have species-specific effects between mouse and rat cells or both. One explanation for this could be higher or more efficient processing by β -secretase, that is expressed at higher levels in neurons than in other cells.¹¹³ Thus, it is possible that any APP increase in neuronal cells was masked by higher rate of processing and the inability to detect the A β 42 peptides via ELISA.

Santana et al have shown that β and γ -secretase activity is unaffected in HSV-1 infected neuroblastoma cells and there is a downregulation of APP cleavage by α -secretase.⁸⁸ We have shown that levels of β -secretase and of the catalytic subunit of γ -secretase (PS2) are not altered in MCMV-infected cells. Similar to what has been shown for HSV-1, we found that MCMV does not induce the activity of β -secretase at 72 HPI (Figure 15). We did not investigate α -secretase, but effects on this enzyme could also lead to increased APP.

The levels of secreted A β 42 in MCMV-infected fibroblasts were similar to uninfected cells (~200 pg/ml); however, detection was a problem with primary neuron samples due to high background from the cell culture media. We did not test intracellular A β levels. The β -secretase enzyme molecules are predominantly localized in endosomes and have been shown to cleave APP within endosomal compartments.¹¹⁴ It has recently been established that A β peptides act as anti-microbial signaling molecules to elicit an

immune response via microglia for CNS infections.^{3,4,26} There is evidence that A β gets sequestered in intracellular autophagic compartments during HSV-1 infection.⁸⁸ Lurain et al showed an increase in intracellular A β 42 staining by immunohistochemistry.¹⁶ There was no apparent decrease in levels of secreted A β 42 from MCMV-infected cells, as one may expect if it was being accumulated intracellularly, unless higher amounts of the peptides were being made. Perhaps MCMV has evolved mechanisms to prevent an increase in A β . Analyses on intracellular A β , especially in neuronal cells, should provide more insight on whether MCMV has effects on A β peptide production or accumulation.

There is also mounting evidence showing that insoluble plaques are not the main factor for cognitive decline but rather diffuse plaques containing soluble A β oligomers.^{25,28,30,47,48} It would be helpful to identify interacting partners for APP and A β using CMV infection as a model system which could lead to elucidation of less known mechanisms for the amyloid pathology in AD. A current, FDA-approved antiviral, foscarnet, was shown to reduce APP accumulation, which sounds promising although it had no effect upon β -secretase activity. Ultimately, analyses of APP and more importantly, A β peptides in animal models are crucial for understanding early steps of AD-specific neurodegeneration.

The changes in the 3 APP isoforms are different so the virus could be upregulating APP at the transcriptional level; however, this requires investigation of various protein-encoding splice variants of APP mRNA. Based on these results, my proposed model (Figure 28) is that MCMV causes accumulation of APP, which might be

less pronounced in neurons with higher APP processing activity. The virus might affect the amyloid pathway differently in rat neuronal cells, but further examination is required. Even if APP is not similarly induced in the neurons, there have been reports that A β peptides secreted from other cells can trigger plaque formation or propagate plaques to neurons.^{29,31,47,49} Infection with MCMV could be a useful model for these mechanisms and therefore these results in tissue culture are promising for future investigations into early steps of AD-related amyloid pathology in mice and rat models.

MCMV AND TAU

It is documented that levels of tau protein are increased in patients with various dementias, including AD.¹⁰⁴ Changes in tau phosphorylation specific to AD during HSV-1 infection, have been studied.¹⁴ These studies used immunohistochemistry, so quantification of total tau and relative sizes remain undetermined. We could not find published studies regarding CMV and tau. We found that similar high molecular weight tau forms (50-250 kDa) were increased in MCMV-infected mouse fibroblasts and rat neuronal cells at 24 to 72 HPI (Figures 17, 21, and 24). We have shown that enhanced phosphorylation of tau at serine 396 occurs during MCMV infection and the hyperphosphorylated tau forms also migrate in those same size ranges of 75 to 250 kDa. This is similar to the study on physiological tau from cerebrospinal fluid of various patients that had different dementias, including AD-specific dementia.¹⁰⁴ These authors found that the higher migrating tau forms were mostly hyperphosphorylated and were detected by antibodies specific for total as well as phosphorylated tau.

When viral late gene expression was inhibited in fibroblasts using foscarnet, total tau protein was not elevated and, in some cases, appeared reduced (Figure 19). Thus, it is possible that MCMV late proteins are involved in induction of total tau and viral immediate-early and/or early proteins may be inhibitory to tau increase. It is established that CMV forms syncytia and extensively remodels the endosomal apparatus as well as the cytoskeleton.¹¹⁵ It is possible that tau phosphorylation is induced by MCMV infection, leading to its dissociation from microtubules, which promotes microtubule remodeling and the cell upregulates tau production to compensate for this.

We used UV-inactivated MCMV to infect fibroblasts, alongside wildtype MCMV infection to confirm that a full viral replication cycle was necessary and to know whether introduction of virion components, which are mainly late gene products, was sufficient to induce tau changes. In the absence of a functional genome and in the presence of virion components, there was no induction of tau seen (Figure 20). This evidence supported that the changes seen in tau were not only due to a delayed cellular response to virion binding and introduction of its components into the cells.

Evidence for tau changes in the rat neuroblastomas and primary cortical neurons was similar to the pattern seen for fibroblasts. This suggests that MCMV infection can be a good system to dissect mechanisms of neurodegeneration. Even though the pattern of tau bands was different in MCMV-infected neuroblastoma cells (Figures 33 and 34 in appendix), there was still enhancement of the slower migrating tau phosphorylated at S396. Multiple tau isoforms might undergo hyperphosphorylation during CMV infection.

Given the size difference of the enhanced bands, it is highly likely that the changes seen are due to numerous sites on tau being significantly modified either by phosphorylation or by other modifications.

We then analyzed phosphorylation at serine 202, as this was another site phosphorylated during HSV-1 infection relevant for AD-related tau.¹⁰³ The phosphorylation was unaffected at this site during MCMV infection. CMV infection can selectively upregulate phosphorylation at a key site involved in AD pathology, i.e. serine 396, but not at serine 202.

Human CMV is known to incorporate host phosphatases in its virion, which are released into the host cell upon infection and lead to global cellular protein hypophosphorylation in infected cells.¹⁰⁷ Also, CMV is known to upregulate host phosphatase activity.¹⁰⁷ The decrease in tau phosphorylation at S396 in the rat B35 cells at 0 HPI (Figure 34 in appendix) is consistent with this evidence and is more apparent in these cells because they have a higher level of phospho-tau (S396) to begin with. In the face of such evidence, based on the strong induction of tau hyperphosphorylation during MCMV infection in our various cell types, we suggest that kinases are more likely to be involved.

It has been shown that HSV-1 can induce levels of GSK3 β and PKA.¹⁰³ GSK3 β can phosphorylate tau at both serine 202 and 396.^{61,105} We tested levels of GSK3 β by western blotting and found that these are not changed during MCMV infection, unlike with HSV-1 (Figure 25). When LiCl treatment was kept throughout the 48 hours of virus

infection, the total tau levels and the phosphorylation at S396 were like those for uninfected cells (Figure 26). When LiCl was added 24 hours after the virus infection had progressed, there were very little changes in the banding patterns for tau and phospho-tau S396. Hence, GSK3 seems to be an unlikely kinase that would primarily mediate the changes in tau forms during MCMV infection. In the presence of LiCl, MCMV was severely inhibited. This may reflect a requirement for GSK3 activity during MCMV infection or LiCl may affect the virus replication through an indirect mechanism.

There may be other targets of GSK3 β that become highly phosphorylated during MCMV infection and that have nothing to do with AD or neurodegeneration. As the phosphorylation at S202 was unaffected, and levels of GSK3 β unaltered during CMV infection, it is highly unlikely that this is a key enzyme involved in hyperphosphorylation of tau in the context of MCMV infection. Other kinases such as PKA, followed by CDK5 and MAPK should be investigated for their role in tau hyperphosphorylation in context of CMV infection.

Considering that MCMV infection has no effect on the steady-state levels of GSK3 β , phosphorylation at S202, and its inhibition does not reverse or prevent tau phosphorylation at S396 or have a major effect on the overall banding pattern of total tau, it is highly likely that GSK3 has very little involvement in tau and its modifications during MCMV infection. Also, the upregulations seen in tau and its modifications are mediated by MCMV late gene products and are absent when the virus is inhibited in presence of

LiCl. This raises interesting possibilities about repurposing existing lithium therapies as novel antivirals.

Herpes viruses establish lifelong latency in their host with periodic reactivation and this may mimic chronic infection leading to overproduction of A β peptides as antimicrobial agents.^{3,4,26} Studies have shown that increased A β can lead to an induction of tau phosphorylation at sites implicated in AD leading to subsequent formation of tau tangles.^{65-67,70,71} However, we have shown that MCMV infection can increase APP (not apparent in neurons) and does not lead to higher level of secreted A β peptide. The increase in tau as well as phosphorylated tau occurs with similar kinetics within 24 to 72 hours. Thus, APP increase does not seem to be required for induction of tau modifications, according to our model (Figure 28).

Based on our data, we suggest that MCMV infection may be a novel system for elucidating modifications of tau and maybe amyloid, in relevant animal models. Unlike animal models of HSV, MCMV can be used in its natural murine host and compared with the closely related permissive rat. Current antivirals can be tested in such models to identify novel preventives for neurodegeneration. Alternatively, drugs containing lithium could be tested for treatment of CMV as potential new antiviral therapies.

REFERENCES

1. Selkoe DJ, Lansbury PJJ. Alzheimer's disease is the most common neurodegenerative disorder. In: *Basic Neurochemistry: molecular, cellular and medical aspects*. Philadelphia, PA Lippincott-Raven; 1999.
2. Bourgade K, Garneau H, Giroux G, et al. beta-Amyloid peptides display protective activity against the human Alzheimer's disease-associated herpes simplex virus-1. *Biogerontology*. 2015;16(1):85-98.
3. Kumar DK, Choi SH, Washicosky KJ, et al. Amyloid-beta peptide protects against microbial infection in mouse and worm models of Alzheimer's disease. *Sci Transl Med*. 2016;8(340):340ra372.
4. Spitzer P, Condic M, Herrmann M, et al. Amyloidogenic amyloid-beta-peptide variants induce microbial agglutination and exert antimicrobial activity. *Sci Rep*. 2016;6:e32228.
5. Ahmed Z, Cooper J, Murray T, et al. A novel in vivo model of tau propagation with rapid and progressive neurofibrillary tangle pathology: the pattern of spread is determined by connectivity, not proximity. *Acta neuropathologica*. 2014;127(5):667-683.
6. Avila J, Lucas JJ, Perez M, Hernandez F. Role of tau protein in both physiological and pathological conditions. *Physiol Rev*. 2004;84(2):361-384.
7. Baas PW, Qiang L. Tau: it's not what you think. *Trends Cell Biol*. 2019;29(6):452-461.
8. Dawson HN, Cantillana V, Jansen M. Loss of tau elicits axonal degeneration in a mouse model of Alzheimer's disease. *Neuroscience*. 2010;169(1):516-531.
9. Schneider LS, Mangialasche F, Andreasen N, et al. Clinical trials and late-stage drug development for Alzheimer's disease: an appraisal from 1984 to 2014. *J Intern Med*. 2014;275(3):251-283.

10. Medina M. An overview on the clinical development of tau-based therapeutics. In: *Int J Mol Sci*. 2018;19:1160.
11. Oxtoby NP, Alexander DC. Imaging plus X: multimodal models of neurodegenerative disease. *Curr Opin Neurol*. 2017;30(4):371-379.
12. Cheeran MC, Lokensgard JR, Schleiss MR. Neuropathogenesis of congenital cytomegalovirus infection: disease mechanisms and prospects for intervention. *Clin Microbiol Rev*. 2009;22(1):99-126.
13. Itzhaki RF, Wozniak MA. Alzheimer's disease and infection: do infectious agents contribute to progression of Alzheimer's disease? *Alzheimer's dementia*. 2010;6(1):83-94.
14. Wozniak MA, Frost AL, Itzhaki RF. Alzheimer's disease-specific tau phosphorylation is induced by herpes simplex type 1. *J Alz dis*. 2009;16(2):341-350.
15. Wozniak MA, Frost AL, Preston CM, Itzhaki RF. Antivirals reduce the formation of key Alzheimer's disease molecules in cell cultures acutely infected with herpes simplex virus type 1. *PLoS One*. 2011;6(10):e25152.
16. Lurain NS, Hanson BA, Martinson J, et al. Virological and immunological characteristics of human cytomegalovirus infection associated with Alzheimer's disease. *J infect dis*. 2013;208(4):564-572.
17. Lin WR, Wozniak MA, Cooper RJ, Wilcock GK, Itzhaki RF. Herpesviruses in brain and Alzheimer's disease. *J Pathol*. 2002;197(3):395-402.
18. Manicklal S, Emery VC, Lazzarotto T, Boppana SB, Gupta RK. The "silent" global burden of congenital cytomegalovirus. *Clin Microbiol Rev*. 2013;26(1):86-102.
19. Cheng SB, Ferland P, Webster P, Bearer EL. Herpes simplex virus dances with amyloid precursor protein while exiting the cell. *PLoS One*. 2011;6(3):e17966.

20. Shipley SJ, Parkin ET, Itzhaki RF, Dobson CB. Herpes simplex virus interferes with amyloid precursor protein processing. *BMC Microbiol.* 2005;5:48.
21. Herrero MT, Morelli M. Multiple mechanisms of neurodegeneration and progression. *Prog Neurobiol.* 2017;155:1.
22. Katsnelson A, De Strooper B, Zoghbi HY. Neurodegeneration: from cellular concepts to clinical applications. *Sci Transl Med.* 2016;8(364):364ps318.
23. ADEAR. Alzheimer's Disease fact sheet. <https://www.nia.nih.gov/health/alzheimers-disease-fact-sheet>. Published 2015. Accessed May 2019.
24. Zhang Y, Thompson R, Zhang H, Xu H. APP processing in Alzheimer's disease. *Molecular brain.* 2011;4,3.
25. Lazarevic V, Fienko S, Andres-Alonso M, et al. Physiological concentrations of amyloid beta regulate recycling of synaptic vesicles via alpha7 acetylcholine receptor and CDK5/calcineurin signaling. *Front Mol Neurosci.* 2017;10:221.
26. Soscia SJ, Kirby JE, Washicosky KJ, et al. The Alzheimer's disease-associated amyloid beta-protein is an antimicrobial peptide. *PLoS One.* 2010;5(3):e9505.
27. O'Brien RJ, Wong PC. Amyloid precursor protein processing and Alzheimer's disease. *Annu Rev Neurosci.* 2011;34:185-204.
28. Gowing E, Roher AE, Woods AS, et al. Chemical characterization of A beta 17-42 peptide, a component of diffuse amyloid deposits of Alzheimer disease. *J Biol Chem.* 1994;269(15):10987-10990.
29. Grothe MJ, Barthel H, Sepulcre J, Dyrba M, Sabri O, Teipel SJ. In vivo staging of regional amyloid deposition. *Neurology.* 2017;89(20):2031-2038.

30. Jansen WJ, Ossenkoppele R, Tijms BM, et al. Association of cerebral amyloid-beta aggregation with cognitive functioning in persons without dementia. *JAMA Psychiatry*. 2018;75(1):84-95.
31. Upadhaya RA, Kosterin I, Kumar S, et al. Biochemical stages of amyloid-beta peptide aggregation and accumulation in the human brain and their association with symptomatic and pathologically preclinical Alzheimer's disease. *Brain*. 2014;137(Pt 3):887-903.
32. Takahashi RH, Milner TA, Li F, et al. Intraneuronal Alzheimer abeta42 accumulates in multivesicular bodies and is associated with synaptic pathology. *Am J Pathol*. 2002;161(5):1869-1879.
33. Ensembl. Gene: APP ENSG00000142192. http://www.ensembl.org/Mus_musculus/Gene/Splice?db=core. Published July 2019. Accessed July 2019.
34. Weidemann A. Identification, biogenesis, and localization of precursors of Alzheimer's disease A4 amyloid protein. *Cell*. 1989;57:115-126.
35. Buxbaum JD, Thinakaran G, Koliatsos V, et al. Alzheimer amyloid protein precursor in the rat hippocampus: transport and processing through the perforant path. *J Neurosci*. 1998;18(23):9629-9637.
36. De Strooper B, Annaert W. Proteolytic processing and cell biological functions of the amyloid precursor protein. *J Cell Sci*. 2000;113(Pt 11):1857-1870.
37. Chen J, Wang M, Turko IV. Quantification of amyloid precursor protein isoforms using quantification concatamer internal standard. *Anal Chem*. 2013;85(1):303-307.
38. Sisodia SS, Koo EH, Hoffman PN, Perry G, Price DL. Identification and transport of full-length amyloid precursor proteins in rat peripheral nervous system. *J Neurosci*. 1993;13(7):3136-3142.

39. Morgan C, Colombres M, Nunez MT, Inestrosa NC. Structure and function of amyloid in Alzheimer's disease. *Prog Neurobiol.* 2004;74(6):323-349.
40. De Strooper B, Vassar R, Golde T. The secretases: enzymes with therapeutic potential in Alzheimer disease. *Nat Rev Neurol.* 2010;6(2):99-107.
41. Holsinger RM, Goense N, Bohorquez J, Strappe P. Splice variants of the Alzheimer's disease beta-secretase, BACE1. *Neurogenetics.* 2013;14(1):1-9.
42. Dominguez D, Tournoy J, Hartmann D, et al. Phenotypic and biochemical analyses of BACE1- and BACE2-deficient mice. *J Biol Chem.* 2005;280(35):30797-30806.
43. Takasugi N, Tomita T, Hayashi I, et al. The role of presenilin cofactors in the gamma-secretase complex. *Nature.* 2003;422(6930):438-441.
44. Hebert SS, Serneels L, DeJaegere T, et al. Coordinated and widespread expression of gamma-secretase in vivo: evidence for size and molecular heterogeneity. *Neurobiol Dis.* 2004;17(2):260-272.
45. Jarrett JT, Berger EP, Lansbury PT, Jr. The carboxy terminus of the beta amyloid protein is critical for the seeding of amyloid formation: implications for the pathogenesis of Alzheimer's disease. *Biochemistry.* 1993;32(18):4693-4697.
46. Dickson DW. The pathogenesis of senile plaques. *J Neuropathol Exp Neurol.* 1997;56(4):321-339.
47. Ferreira ST, Vieira MN, DeFelice FG. Soluble protein oligomers as emerging toxins in Alzheimer's and other amyloid diseases. *IUBMB Life.* 2007;59(4-5):332-345.
48. Lacor PN, Buniel MC, Chang L, et al. Synaptic targeting by Alzheimer's-related amyloid beta oligomers. *J Neurosci.* 2004;24(45):10191-10200.
49. Corbett GT, Buss EW. Non-neuronal cells exacerbate beta-amyloid aggregation in the aged brain. *J Neurosci.* 2014;34(30):9825-9827.

50. Mandelkow E, Mandelkow E-M. Microtubules and microtubule associated proteins. *Curr Opin Cell Biol.* 1995;7(1):72-81.
51. Mandell JW, Banker GA. A spatial gradient of tau protein phosphorylation in nascent axons. *J Neurosci.* 1996;16(18):5727-5740.
52. Buee L. Tau protein isoforms, phosphorylation and role in neurodegenerative disorders. *Brain Res Rev.* 2000;33:95-130.
53. Martin L, Latypova X, Terro F. Post-translational modifications of tau protein: implications for Alzheimer's disease. *Neurochem Int.* 2011;58(4):458-471.
54. Alonso AD, Di Clerico J, Li B, et al. Phosphorylation of tau at Thr212, Thr231, and Ser262 combined causes neurodegeneration. *J Biol Chem.* 2010;285(40):30851-30860.
55. Tapia-Rojas C, Cabezas-Opazo F, Deaton CA, Vergara EH, Johnson GVW, Quintanilla RA. It's all about tau. *Prog Neurobiol.* 2019;175:54-76.
56. Varghese M, Santa-Maria I, Ho L, et al. Extracellular tau paired helical filaments differentially affect tau pathogenic mechanisms in mitotic and post-mitotic cells: implications for mechanisms of tau propagation in the brain *J Alzheimers Dis.* 2016;54(2):477-496.
57. Ando K, Maruko-Otake A, Ohtake Y, Hayashishita M, Sekiya M, Iijima KM. Stabilization of microtubule-unbound tau via tau phosphorylation at ser262/356 by par-1/MARK contributes to augmentation of ad-related phosphorylation and abeta42-induced tau toxicity. *PLoS Genet.* 2016;12(3):e1005917.
58. Valeriy D. Identification of the sites of tau hyperphosphorylation and activation of tau kinases in synucleinopathies and Alzheimer's diseases. *PLoS One.* 2013;8(9):e75025.
59. Cavallini A, Brewerton S, Bell A, et al. An unbiased approach to identifying tau kinases that phosphorylate tau at sites associated with Alzheimer disease. *J Biol Chem.* 2013;288(32):23331-23347.

60. Benneceb M, Gong CX, Grundke-Iqbal I, Iqbal K. Role of protein phosphatase-2A and -1 in the regulation of GSK-3, cdk5 and cdc2 and the phosphorylation of tau in rat forebrain. *FEBS Lett.* 2000;485(1):87-93.
61. Liu SJ, Zhang JY, Li HL, et al. Tau becomes a more favorable substrate for GSK-3 when it is prephosphorylated by PKA in rat brain. *J Biol Chem.* 2004;279(48):50078-50088.
62. Rahman A, Grundke-Iqbal I, Iqbal K. PP2B isolated from human brain preferentially dephosphorylates ser-262 and ser-396 of the Alzheimer disease abnormally hyperphosphorylated tau. *Journal of neural transmissions (Vienna).* 2006;113(2):219-230.
63. Kovacs GG. Tauopathies. *Handb Clin Neurol.* 2017;145:355-368.
64. Theendakara V, Bredesen DE, Rao RV. Downregulation of protein phosphatase 2A by apolipoprotein E: Implications for Alzheimer's disease. *Mol Cell Neurosci.* 2017;83:83-91.
65. Bennett RE, DeVos SL, Dujardin S, et al. Enhanced Tau Aggregation in the Presence of Amyloid beta. *Am J Pathol.* 2017;187(7):1601-1612.
66. Farizatto KLG, Ikonne US, Almeida MF, Ferrari MFR, Bahr BA. Abeta42-mediated proteasome inhibition and associated tau pathology in hippocampus are governed by a lysosomal response involving cathepsin B: Evidence for protective crosstalk between protein clearance pathways. *PLoS One.* 2017;12(8):e0182895.
67. Hu X, Li X, Zhao M, Gottesdiener A, Luo W, Paul S. Tau pathogenesis is promoted by Abeta1-42 but not Abeta1-40. *Mol Neurodegener.* 2014;9:52.
68. Oliveira JM, Henriques AG, Martins F, Rebelo S, Cruz e Silva OA. Amyloid-beta modulates both abetaPP and tau phosphorylation. *J Alzheimers Dis.* 2015;45(2):495-507.

69. Inbar D, Belinson H, Rosenman H, Michaelson DM. Possible role of tau in mediating pathological effects of apoE4 in vivo prior to and following activation of the amyloid cascade. *Neurodegener Dis.* 2010;7(1-3):16-23.
70. Nisbet RM, Polanco JC, Ittner LM, Gotz J. Tau aggregation and its interplay with amyloid-beta. *Acta Neuropathol.* 2015;129(2):207-220.
71. Pallo SP, DiMaio J, Cook A, Nilsson B, Johnson GVW. Mechanisms of tau and Abeta-induced excitotoxicity. *Brain Res.* 2016;1634:119-131.
72. Rapoport M, Dawson HN, Binder LI, Vitek MP, Ferreira A. Tau is essential to beta - amyloid-induced neurotoxicity. *Proc Natl Acad Sci U S A.* 2002;99(9):6364-6369.
73. Ittner A, Chua SW, Bertz J, et al. Site-specific phosphorylation of tau inhibits amyloid-beta toxicity in Alzheimer's mice. *Science.* 2016;354(6314):904-908.
74. Whitley R. *Medical microbiology 4th edition: chapter 68 - Herpesviruses.* University of Texas Medical Branch at Galveston; 1996.
75. Whitley RJ. Herpesviruses. In: University of Texas Medical Branch at Galveston; 1996: <https://www.ncbi.nlm.nih.gov/pubmed/>. Accessed 1996.
76. Foulon T. Herpesviridae: classification and structure in 1991. *Comp Immunol Microbiol Infect Dis.* 1992;15(1):13-29.
77. Grinde B. Herpesviruses: latency and reactivation – viral strategies and host response. In: *J Oral Microbiol.* 2013;5.
78. Jackson JW, Sparer T. There is always another way! cytomegalovirus' multifaceted dissemination schemes. *Viruses.* 2018;10(7).
79. Honess RW, Roizman B. Regulation of herpesvirus macromolecular synthesis. I. Cascade regulation of the synthesis of three groups of viral proteins. *J Virol.* 1974;14(1):8-19.

80. Geballe AP, Leach FS, Mocarski ES. Regulation of cytomegalovirus late gene expression: gamma genes are controlled by posttranscriptional events. *J Virol.* 1986;57(3):864-874.
81. Kalejta RF. Tegument proteins of human cytomegalovirus. *Microbiol Mol Biol Rev.* 2008;72(2):249-265.
82. Agelidis AM, Shukla D. Cell entry mechanisms of HSV: what we have learned in recent years. *Future Virol.* 2015;10(10):1145-1154.
83. Booth JC, Beesley JE, Stern H. Syncytium formation caused by human cytomegalovirus in human embryonic lung fibroblasts. *Arch Virol.* 1978;57(2):143-152.
84. Kammerman EM, Neumann DM, Ball MJ, Lukiw W, Hill JM. Senile plaques in Alzheimer's diseased brains: possible association of beta-amyloid with herpes simplex virus type 1 (HSV-1) L-particles. *Medical hypotheses.* 2006;66(2):294-299.
85. Letenneur L, Peres K, Fleury H, et al. Seropositivity to Herpes Simplex Virus Antibodies and Risk of Alzheimer's Disease: A Population-Based Cohort Study. 2008.
86. Readhead B, Haure-Mirande JV, Funk CC, et al. Multiscale analysis of independent alzheimer's cohorts finds disruption of molecular, genetic, and clinical networks by human herpesvirus. *Neuron.* 2018;99(1):64-82.
87. Braun E, Zimmerman T, Hur TB, et al. Neurotropism of herpes simplex virus type 1 in brain organ cultures. *J Gen Virol.* 2006;87(Pt 10):2827-2837.
88. Santana S, Recuero M, Bullido MJ, Valdivieso F, Aldudo J. Herpes simplex virus type I induces the accumulation of intracellular beta-amyloid in autophagic compartments and the inhibition of the non-amyloidogenic pathway in human neuroblastoma cells. *Neurobiol Aging.* 2012;33(2):430.e419-433.

89. Dasgupta G, BenMohamed L. Of mice and not humans: how reliable are animal models for evaluation of herpes CD8+-T cell-epitopes-based immunotherapeutic vaccine candidates *Vaccine*. 2011;29(35):5824-5836.
90. Webre JM, Hill JM, Nolan NM, et al. Rabbit and mouse models of HSV-1 latency, reactivation, and recurrent eye diseases. *Journal of Biomedicine and Biotechnology*. 2012;18.
91. Devanand D. Anti-viral Therapy in Alzheimer's Disease. NIH U.S. National Library of Medicine. <https://clinicaltrials.gov/ct2/show/NCT03282916>. Published 2019. Updated April 11, 2019. Accessed July 17, 2019.
92. Jackson SE, Redeker A, Arens R, et al. CMV immune evasion and manipulation of the immune system with aging. *Geroscience*. 2017;39(3):273-291.
93. Rawlinson WD, Farrell HE, Barrell BG. Analysis of the complete DNA sequence of murine cytomegalovirus. *J Virol*. 1996;70(12):8833-8849.
94. Smith CB, Wei LS, Griffiths M. Mouse cytomegalovirus is infectious for rats and alters lymphocyte subsets and spleen cell proliferation. *Archives of virology*. 1986;90:313-323.
95. Hanson LK, Slater JS, Karabekian Z, et al. Replication of murine cytomegalovirus in differentiated macrophages as a determinant of viral pathogenesis. *J Virol*. 1999;73(7):5970-5980.
96. Seifert JL, Som S, Hynds DL. Differential activation of rac1 and rhoA in neuroblastoma cell fractions. *Neurosci Lett*. 2009;450(2):176-180.
97. Hanson LK, Dalton BL, Cageao LF, et al. Characterization and regulation of essential murine cytomegalovirus genes m142 and m143. *Virology*. 2005;334(2):166-177.
98. Crumpacker CS. Mechanism of action of foscarnet against viral polymerases. *Am J Med*. 1992;92(2a):3s-7s.

99. Roche. DIG application manual for filter hybridization. In: Seth DEO, Grünewald-Janho S, Kruchen B, Rüger B, eds. Germany: Roche Diagnostics GmbH; 2008.
100. GeneCopoeia I. Total RNA isolation protocol. In: GeneCopoeia, Inc.; 2013.
101. Bell G. Quantifying western blots: none more black. In: *BMC Biol.* 2016;14:116.
102. Evans DB, Rank KB, Bhattacharya K, Thomsen DR, Gurney ME, Sharma SK. Tau phosphorylation at serine 396 and serine 404 by human recombinant tau protein kinase II inhibits tau's ability to promote microtubule assembly. *J Biol Chem.* 2000;275(32):24977-24983.
103. Wozniak M, Frost A, Itzhaki R. Alzheimer's disease-specific tau phosphorylation is induced by herpes simplex type 1. *Journal of Alzheimer's disease.* 2009;16(2):341-350.
104. Sjogren M, Davidsson P, Tullberg M, et al. Both total and phosphorylated tau are increased in Alzheimer's disease. *J Neurol Neurosurg Psychiatry.* 2001;70(5):624-630.
105. Utton MA, Vandecandelaere A, Wagner U, et al. Phosphorylation of tau by glycogen synthase kinase 3beta affects the ability of tau to promote microtubule self-assembly. *Biochem J.* 1997;323(Pt 3):741-747.
106. Kimura T, Ono T, Takamatsu J, et al. Sequential changes of tau-site-specific phosphorylation during development of paired helical filaments. *Dementia.* 1996;7(4):177-181.
107. Hakki M, Geballe AP. Cellular serine/threonine phosphatase activity during human cytomegalovirus infection. *Virology.* 2008;380(2):255-263.
108. Noble W, Planel E, Zehr C, et al. Inhibition of glycogen synthase kinase-3 by lithium correlates with reduced tauopathy and degeneration in vivo. *Proc Natl Acad Sci U S A.* 2005;102(19):6990-6995.

109. Ziaie Z, Brinker JM, Kefalides NA. Lithium chloride suppresses the synthesis of messenger RNA for infected cell protein-4 and viral deoxyribonucleic acid polymerase in herpes simplex virus-1 infected endothelial cells. *Lab Invest.* 1994;70(1):29-38.
110. Skinner GR, Hartley C, Buchan A, Harper L, Gallimore P. The effect of lithium chloride on the replication of herpes simplex virus. *Med Microbiol Immunol.* 1980;168(2):139-148.
111. Ziaie Z, Kefalides NA. Lithium chloride restores host protein synthesis in herpes simplex virus-infected endothelial cells. *Biochem Biophys Res Commun.* 1989;160(3):1073-1078.
112. Van Den Pol AN, Vieira J, Spencer DD, Santarelli JG. Mouse cytomegalovirus in developing brain tissue: analysis of 11 species with GFP-expressing recombinant virus. *J Comp Neurol.* 2000;427(4):559-580.
113. Vassar R, Bennett BD, Babu-Khan S, et al. Beta-secretase cleavage of Alzheimer's amyloid precursor protein by the transmembrane aspartic protease BACE. *Science.* 1999;286(5440):735-741.
114. Chia PZ, Toh WH, Sharples R, Gasnereau I, Hill AF, Gleeson PA. Intracellular itinerary of internalised beta-secretase, BACE1, and its potential impact on beta-amyloid peptide biogenesis. *Traffic.* 2013;14(9):997-1013.
115. Das S, Vasanji A, Pellett PE. Three-dimensional structure of the human cytomegalovirus cytoplasmic virion assembly complex includes a reoriented secretory apparatus. *J Virol.* 2007;81(21):11861-11869.
116. McKusick V, Hamosh A. OMIM 104760-Amyloid beta A4 precursor protein; APP. 2019.

APPENDIX A
LEVELS OF APP IN RAT B35 NEUROBLASTOMAS

We tested steady-state levels of APP in rat B35 neuroblastomas because the results were different in mouse NIH3T3 fibroblasts and primary RCN. We wanted to determine whether this difference was because the fibroblasts are semi-transformed cells while the neurons are not. The Figure below shows the western blots for APP (17A) in uninfected and MCMV-infected B35 cells, followed by the densitometric analysis of individual APP isoforms (28B). The results for the B35 cells were more like the RCN, so the difference between fibroblasts and RCN is unlikely due to the semi-transformed nature of the fibroblasts and more likely are due to cell-type or species.

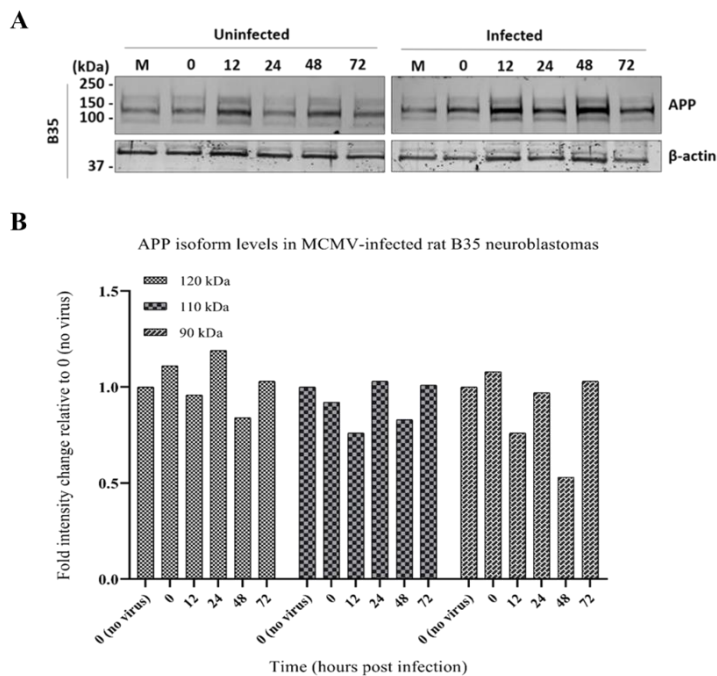


Figure 29. MCMV infection does not induce APP in rat B35 neuroblastomas. (A) Western blots showing APP in uninfected and infected neuroblastoma cells through 72 HPI. (B) For infected cells, levels of each of the 3 APP isoforms detected were quantitated with scanning densitometry, normalized against β -actin, and all time points compared to 0 hours sample without virus. Data were plotted as fold intensity change relative to 0 (no virus).

APPENDIX B

LEVELS OF PS2 IN RAT PRIMARY CORTICAL NEURONS (RCN)

We analyzed whether MCMV infection changed steady-state levels of PS2, the active subunit of γ -secretase in primary RCN. On the western blot, there was a darker band at 12 HPI for infected RCN (Figure 30). This result is largely consistent with that seen in fibroblasts and there is not much evidence of a change. More experiment repetitions are required to confirm whether this is a consistent pattern seen during MCMV infection at 12 HPI.

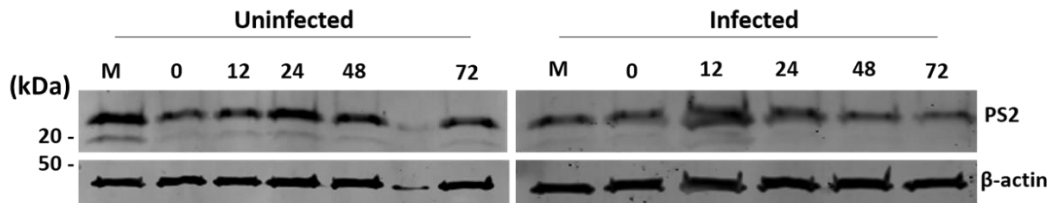


Figure 30. Levels of PS2 in RCN during MCMV infection. (A) Western blots showing PS2 levels in uninfected and MCMV-infected RCN. (B) Densitometric analyses of PS2 levels. Densitometry values were normalized for equal loading against β -actin. Level for 0 hours without virus was set as 1.0 and all time points compared to this.

APPENDIX C

SECRETED AB42 IMMUNOBLOTTING ANALYSES

We analyzed for amounts of secreted A β 42 peptide in media taken from MCMV-infected fibroblasts and primary neurons. The sensitivity of detection was first analyzed by blotting different concentrations of synthetic A β 42 peptide (Figure 31). The synthetic peptide was dissolved in DMEM-10% BCS media and 10-fold serial dilutions were made. These were subjected to denaturing polyacrylamide gel electrophoresis on 15-18% resolving gels followed by western blotting with rabbit monoclonal anti-A β 42 antibody, detected by goat anti-rabbit 800.

We could successfully detect concentrations ranging from 1 μ g down to 0.1 ng or 100 pg of A β 42 peptide by this method. We then performed western blot analysis using 60 μ l of supernatant taken from fibroblast cultures that were uninfected and infected with MCMV (MOI 2 PFU/cell) with 18% polyacrylamide gels. and subjected them to western blotting. We were unable to detect A β 42 peptide in our samples (Figure 31). We concluded that concentrations of secreted amyloid beta peptide must be lower than 100 pg/60 μ l in our samples. A more sensitive technique was required. We included media from rat cortical neuron cultures for this gel as amyloid is known to be expressed at a higher level in neuronal cells where it functions as a signaling molecule²⁵. We were unable to detect secreted A β 42 in these samples as well. The concentration would need to be about 1700 pg/ml for successful detection. From our ELISA, we found that background readings from sterile media were around 250-300 pg/ml and the secreted peptide levels must have been lower than this. That would explain why we could not detect the peptides from neuronal cells on our western blots.

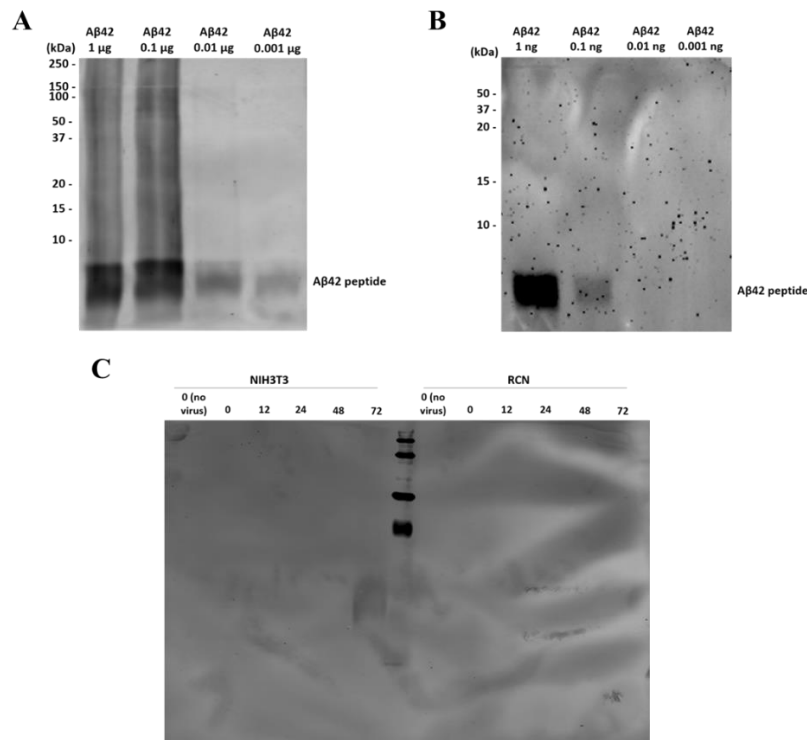


Figure 31. Secreted Aβ42 peptide detection via western blotting (A) Synthetic Aβ42 peptide was diluted to 1, 0.1, 0.01, and 0.001 μg in fibroblast culture medium, samples were loaded onto a 15% resolving polyacrylamide gel before transfer to nitrocellulose membranes. (B) Synthetic Aβ42 peptide was diluted to 1, 0.1, 0.01, and 0.001 ng in fibroblast culture medium, run on 18% resolving polyacrylamide gel before transfer to nitrocellulose. Membranes were blocked in 5% milk, probed with rabbit anti-Aβ42 (CST), and detected with goat anti-rabbit 800 secondary antibody on a LiCor Odyssey CLx. (C) Conditioned media from fibroblasts and rat cortical neurons. Protein ladder dark bands are 50, 37, 20, and 15 kDa from top to bottom of blot.

APPENDIX D
NORTHERN BLOT EXPERIMENTS

We hypothesized that upregulation of APP by MCMV may start at the mRNA level. The amyloid beta precursor protein gene is transcribed into more than 8 protein-encoding alternative splice variants¹¹⁶. As there were differences in the levels of the 3 protein isoforms, we investigated which of the splice variants may be upregulated during infection. We performed northern blots using a DIG-labeled probe containing part of the sequence for APP exon 4 on total RNA isolated from uninfected and infected fibroblasts.

The fragment for the probe was generated via HindIII and Sall restriction enzyme digestion of the plasmid pEGFP-n1-APP (Addgene, #69924) followed by gel extraction and was DIG labeled. Total RNA was extracted using RNazol and separated out on a 1% agarose gel containing 2% formaldehyde (Figure 29). As the expected sizes of APP transcripts ranged from 0.3 kbp to 3.7 kbp (Ensembl gene ENSG00000084234), the agarose-formaldehyde gel was subjected to partial alkaline hydrolysis before transfer of nucleic acid onto nylon membranes. Successful transfer was confirmed by visual detection of ethidium bromide-stained rRNA and RNA ladder on the membranes using a UV transilluminator (data not shown). After blocking and probing, no signal for any lanes was detected. When these experiments were repeated with varying conditions, there was still no improvement. This could be due to colorimetric detection being less sensitivity than using radioactive probes or chemiluminescence.

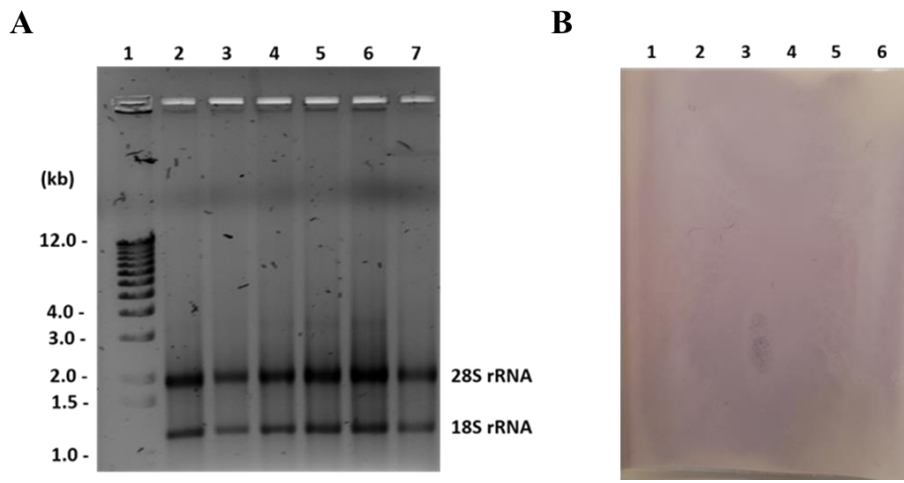


Figure 32. Northern blot analysis of total RNA isolated from MCMV-infected fibroblasts. (A) Agarose gel showing total RNA isolated from NIH3T3 cells. Lane 1 is the molecular weight ladder (kb – kilobases), lane 2 – 0-no virus, lane 3 – 0 HPI, lane 4 – 12 HPI, lane 5 – 24 HPI, lane 6 – 48 HPI, lane 7 – 72 HPI. (B) Nylon membrane after colorimetric detection of DIG-labeled APP probe applied to NIH3T3 RNA samples. Lanes 1 through 6 correspond with lanes 2 to 7 of gel shown in A. Successful transfer of RNA to nylon membrane was confirmed visually by holding the membrane above a UV transilluminator and checking for ethidium bromide fluorescence.

APPENDIX E

TAU AND ITS MODIFICATIONS IN MCMV-INFECTED RAT B35 CELLS

We analyzed total tau levels and tau phosphorylation at S396 and S202 in B35 neuroblastomas as previous studies with HSV-1 infection were performed in human neuroblastoma cells^{14,15}. We wanted to investigate whether MCMV, another herpesvirus, could induce tau and its modifications like those seen with HSV-1 infection.

We found that there is an enhancement of tau forms of 50-250 kDa size at 48 and 72 HPI compared to uninfected cells at the same time points (Figure 30A). However, the pattern of tau upregulation was more subtle than that seen in fibroblasts and primary neurons. There were fewer intense bands ranging from 100 to 250 kDa, unlike those seen in MCMV-infected fibroblasts. Clearly, MCMV is able to mediate an increase in tau at late times of infection across a variety of cell types.

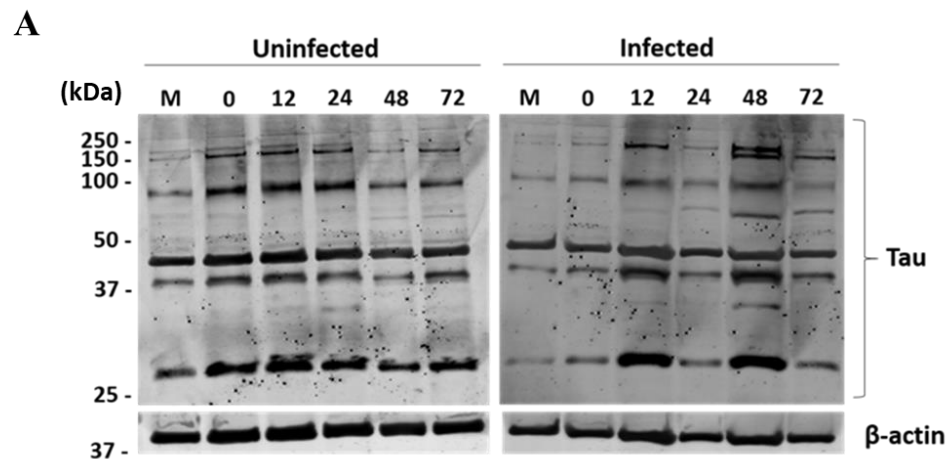


Figure 33: Rat B35 neuroblastomas have induced tau during MCMV infection. Western blots showing total tau over 72 hours with and without MCMV infection rat B35 neuroblastoma cells. M – mock infected.

We analyzed tau phosphorylation at S396 in B35 cells. Like the fibroblasts and primary neurons, there was an enhancement of ~100-150 kDa tau forms at 48 and 72 HPI (Figure 34A). Hence, MCMV can induce tau phosphorylation at S396 at late time points in fibroblasts and neuronal cells. There was no detectable phosphorylation at S202 with or without MCMV infection (Figure 34B). This was different than what was published for HSV-1 infected neuroblastoma cells where phosphorylation at S202 was higher.¹⁴ It was also different than the fibroblasts and primary neurons where phosphorylation was present, but it was unaltered in presence of MCMV. It may be because these are tumor-derived cells.

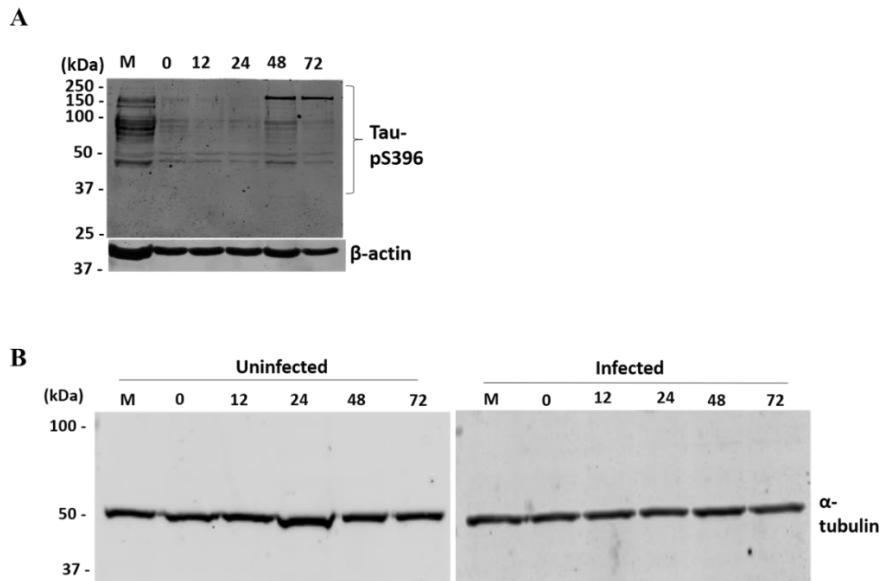


Figure 34. Tau phosphorylation in rat B35 neuroblastoma cells. (A) Western blot showing tau phosphorylated at S396 during MCMV infection over 72 hours. (B) Western blots showing tau phosphorylated at S202 in uninfected and MCMV-infected cells over 72 hours. M – mock infected.